

Enhancing xURLLC with RSMA-Assisted Massive-MIMO Networks: Performance Analysis and Optimization

Yuang Chen, *Student Member, IEEE*, Hancheng Lu, *Senior Member, IEEE*, Chenwu Zhang, Yansha Deng, *Senior Member, IEEE*, and Arumugam Nallanathan, *Fellow, IEEE*

Abstract—Massive interconnection has sparked people’s envisioning for next-generation ultra-reliable and low-latency communications (xURLLC), prompting the design of customized next-generation advanced transceivers (NGAT). Rate-splitting multiple access (RSMA) has emerged as a pivotal technology for NGAT design, given its robustness to imperfect channel state information (CSI) and resilience to quality of service (QoS). Additionally, xURLLC urgently appeals to large-scale access techniques, thus massive multiple-input multiple-output (mMIMO) is anticipated to integrate with RSMA to enhance xURLLC. In this paper, we develop an innovative RSMA-assisted massive-MIMO xURLLC (RSMA-mMIMO-xURLLC) network architecture tailored to accommodate xURLLC’s critical QoS constraints in finite blocklength (FBL) regimes. Leveraging uplink pilot training under imperfect CSI at the transmitter, we estimate channel gains and customize linear precoders for efficient downlink short-packet data transmission. Subsequently, we formulate a joint rate-splitting, beamforming, and transmit antenna selection optimization problem to maximize the total effective transmission rate (ETR). Addressing this multi-variable coupled non-convex problem, we decompose it into three corresponding subproblems and propose a low-complexity joint iterative algorithm for efficient optimization. Extensive simulations substantiate that compared with non-orthogonal multiple access (NOMA) and space division multiple access (SDMA), the developed architecture improves the total ETR by 15.3% and 41.91%, respectively, as well as accommodates larger-scale access.

Index Terms—Next-generation ultra-reliable low-latency communications (xURLLC), rate-splitting multiple access (RSMA), massive multiple-input multiple-output (mMIMO), finite blocklength (FBL).

I. INTRODUCTION

A. Background

The rapid evolution of the sixth-generation wireless networks (6G) has propelled the advent of the internet-of-everything (IoE) and indisputably catalyzed the advancement of ultra-reliable and low-latency communications (URLLC) [1–5]. URLLC endeavors to accomplish scalability and ultra-reliability with low latency [1, 2], prompting the continuous emergence of high-stack control and mission-critical applications across vertical sectors, such as extended reality, brain-machine interfaces, robotic control, and industrial automation [1–4]. These applications have provoked unprece-

ded demands for stringent quality-of-service (QoS), fueling the anticipation among stakeholders for the next-generation URLLC (xURLLC). To this end, the design of customized next-generation advanced transceivers (NGAT) is pivotal for implementing xURLLC, which necessitates exceptional scalability, robust multiple access, flexible interference management, elastic low latency, and impeccable reliability [3, 4, 6, 7].

The predominant roadmap to fulfill low latency for xURLLC involves orchestrating extensive short-packet data transmissions within dynamic wireless networks [8]. Finite blocklength (FBL) is essential to guarantee compliance with low-latency prerequisites [2–4], rendering Shannon’s capacity theory inadequate due to non-negligible decoding error probability (DEP) in FBL regimes [3, 4, 9]. To rectify this theoretical deficiency, finite blocklength coding theory has emerged, revealing the maximum achievable data rate for short-packet data transmissions while highlighting the intricate tradeoff between DEP and target latency. This tradeoff is not solely determined by blocklength but is also impacted by transmit power, transmission rate, channel state information (CSI), antenna amounts, and device scale [2, 3]. To meet xURLLC’s QoS requirements, there arises the imminent necessity for innovative multi-access techniques to customize xURLLC’s NGAT, which must deliver higher spectral efficiency (SE), greater energy efficiency (EE), more flexible interference management, wider coverage, and larger effective transmission rates (ETR) [1–3, 6, 7].

Rate-splitting multiple access (RSMA) has emerged as a transformative multi-access technique, revolutionizing the architectural design and bolstering massive access, non-orthogonal transmission, and flexible interference management for 6G [6, 7, 10]. It introduces a promising paradigm at the physical layer, expected to be exploited in the design of NGAT for xURLLC [1, 3, 6, 7]. The fundamental principle of RSMA involves splitting the intended message for receivers into common and private parts, combining common parts into a super common message encoded using a shared codebook while encoding each receiver’s private part independently using a distinct private codebook [6, 7]. These streams are transmitted leveraging linear precoding, enabling non-orthogonal transmission within the same time-frequency resources [6, 7, 10]. By exploiting rate-splitting, RSMA can *partially decode the interference and partially treat the interference as noise* [6, 7], striking a balance between fully decoding interference and treating interference as noise [6, 7]. Therefore, RSMA stands as a pivotal technique for advancing xURLLC.

Yuang Chen, Hancheng Lu, and Chengwu Zhang are with the CAS Key Laboratory of Wireless-Optical Communications, School of Information Science and Technology, University of Science and Technology of China, Hefei 230027, China (email: yuangchen21@mail.ustc.edu.cn; hclu@ustc.edu.cn; cwzhang@mail.ustc.edu.cn). Yansha Deng is with King’s College London (email: yansha.deng@kcl.ac.uk); Arumugam Nallanathan is with Queen Mary University of London (email: a.nallanathan@qmul.ac.uk).

B. Research Motivations and Challenges

Although RSMA has demonstrated its potential to enhance QoS in wireless networks [11–13], the research centered on the integration of RSMA into xURLLC remains in its nascent stages, accompanied by numerous unprecedented challenges. On the one hand, RSMA’s capability to facilitate flexible interference management for receivers involves cumbersome message splitting and combining processes, which come at the expense of increasing framework complexity, posing formidable challenges for seamlessly integrating with other advanced technologies, like massive-MIMO [14], grant-free access [15], and FBL regime [6]. On the other hand, the optimal rate-splitting and beamforming schemes in complex wireless environments, especially under the FBL and massive-MIMO scenarios, are no simple feat [6, 7]. Additionally, for user terminals to successfully decode and eliminate common and private messages at receivers leveraging successive interference cancellation (SIC) techniques, user terminals must possess knowledge of RSMA splitting and combining short-packet messages at the transmitter. However, since the extremely complex integration architecture of xURLLC and RSMA, this remains an unresolved challenge.

The predominant claim of xURLLC center on supporting the rapidly proliferating device connectivity while meeting stringent QoS demands. Despite RSMA’s potential to enhance xURLLC [3, 4, 13], addressing massive access remains a imminent challenge [6, 7]. Massive MIMO (mMIMO) emerges as a promising solution, boasting advantages like enhanced spectral efficiency (SE) and energy efficiency (EE) by over tenfold and a hundredfold, respectively [16, 17]. However, integrating RSMA with mMIMO is confronted with several unexploited challenges. Firstly, RSMA-assisted mMIMO (RSMA-mMIMO) systems rely heavily on spatial multiplexing, demanding accurate channel knowledge for the transceiver’s reliable uplink and downlink transmissions. Secondly, effective beamforming and interference management of RSMA-mMIMO systems hinges on precise CSIT, which is typically unavailable in practical scenarios, leading to potential multi-user interference and compromised latency and reliability. Finally, transmit antenna selection of RSMA-mMIMO systems demands judicious deliberation to avoid escalating hardware costs, power consumption [18], signal processing complexity [19], compromised SE [16], and interference and DEP sensitivity [20]. Therefore, tailoring an innovative RSMA-mMIMO system for xURLLC necessitates meticulous study to imperfect CSIT in channel estimation, interference management, transmit antenna selection, and resource allocation schemes.

C. Related Work

Sate-of-the-art research endeavors have extensively focused on optimizing short-packet transmission for xURLLC [3, 4, 21, 22]. Our prior work has developed an xURLLC-enabled multi-user MIMO network to minimize the upper-bounded statistical delay violation probability by jointly optimizing the pilot length and precoding matrix [3]. FBL-based short packets with sporadic arrival traffic necessitate tail distribution exploration. For this reason, Y. Chen *et al.* in [4] have proposed a non-orthogonal multiple access (NOMA)-assisted uplink xURLLC network that incorporates a theoretical framework

for tail analysis. Joint design algorithms for channel training and data transmission have presented formidable challenges in rigorous reliability and FBL regimes, leading to proposing a low-complexity joint design framework for MIMO-enabled URLLC networks [21]. Moreover, a unified semi-blind detection framework has been proposed to facilitate massive access for xURLLC, enhancing scalability, reliability, and latency tradeoffs [22].

RSMA has emerged as a pioneering multi-access technology to enhance xURLLC’s QoS provisioning. Research has thoroughly explored the intricate relationship between the sum rate and blocklength of RSMA-assisted URLLC, addressing various network loads and user deployment scenarios [11]. Notably, RSMA endows with the capability to guarantee user fairness in both underloaded and overloaded deployment paradigms [23]. Authors in [12] have proposed a novel non-cooperative/cooperative multi-group multicast deployment model to maximize the minimum group rate for URLLC networks. To fulfill xURLLC’s stringent QoS requirements, authors in [13] have investigated a multi-reconfigurable intelligent surface (RIS)-assisted RSMA architecture, aiming to prompt enhanced SE and maximize the sum throughput. Additionally, an innovative cooperative RSMA framework in a two-layer heterogeneous network has been proposed, which leverages users with favorable channel quality as full-duplex relays to assist users with weaker signals [24].

Extensive studies have explored performance enhancements in RSMA-mMIMO networks [14, 23, 25, 26]. A novel RSMA-based massive-MIMO system has been proposed to analyze the implications of channel aging, spatial correlation, and Rician factor [14]. The delay between CSI acquisition and data transmission stands as the primary factor contributing to imperfect CSIT. Authors in [25] have derived the lower bound of the ergodic sum rate and investigated the optimal power allocation for common and private streams. To address concerns about long-term electromagnetic (EM) radiation exposure, RSMA has been applied to enhance SE and EE of uplink massive MIMO while rigorously constraining EM exposure [26]. Leveraging the polarization domain for additional degrees of freedom (DoF), authors in [23] have improved the successive interference cancellation (SIC) performance and developed three dual-polarized downlink transmission strategies for RSMA-mMIMO systems.

D. Main Contributions

To effectively address the aforementioned challenges, we propose an innovative RSMA-assisted massive-MIMO xURLLC (RSMA-mMIMO-xURLLC) network, which has been demonstrated unequivocally furnish exceptional QoS provisioning for xURLLC. We adopt the ETR as a performance indicator to evaluate the relationship between the achievable data rate and xURLLC’s QoS requirements. Subsequently, we formulate a joint rate-splitting, beamforming, and transmit antenna selection optimization problem to maximize the total ETR. To efficiently solve this problem, we propose a novel joint optimization mechanism to decompose the original problem into three corresponding subproblems. Furthermore, a low-complexity joint iterative optimization algorithm is designed to efficiently alternate the optimization of power allocation, rate-

splitting, and transmit antenna selection, respectively. Exhaustive experiments substantiate the extraordinary performance of the developed RSMA-mMIMO-xURLLC network compared to several state-of-the-art multi-access frameworks. The main contributions of this paper are summarized as follows:

- We develop an innovative RSMA-mMIMO-xURLLC network architecture, where the transceiver is equipped with multiple antennas to fully exploit the potential of RSMA-mMIMO systems. The imperfect CSIT and the FBL regime have been accounted for meticulously accommodating xURLLC's critical QoS requirements. Moreover, uplink pilot training has been undertaken to estimate channel gains, and the linear precoder has been tailored for efficient downlink short-packet data transmission.
- We derive closed-form expressions for the signal-to-interference-plus-noise ratios (SINRs) of common and private streams, as well as the corresponding channel capacity. Subsequently, we formulate a joint rate-splitting, beamforming, and transmit antenna selection optimization problem to maximize the total ETR. To effectively overcome this problem, we reformulate it by profoundly exploring the relationships between SINRs of common and private streams with antenna amounts, large-scale fading, transmit power, blocklength, and channel estimation quality (CEQ).
- We decompose the reformulated problem into three corresponding subproblems. In particular, the successive convex approximation (SCA)-based algorithm is proposed to solve the power allocation subproblem, while the rate-splitting subproblem is effectively addressed by interior-point methods. Furthermore, the transmit antenna selection subproblem is equivalently transformed into a one-dimensional integer search problem. Ultimately, a low-complexity joint iterative optimization algorithm is proposed to efficiently alternate the optimization of these three subproblems.
- Extensive simulations substantiate the optimality and convergence performance of the proposed joint iterative optimization algorithm. Additionally, compared with the state-of-the-art multi-access schemes, including NOMA, and space division multiple access (SDMA), the extraordinary performance of our developed RSMA-mMIMO-xURLLC network architecture can be demonstrated in terms of ETR, reliability, latency, and robustness for xURLLC.

The remainder of this paper is organized as follows. In Sec. II, the RSMA-mMIMO-xURLLC network architecture is investigated. Sec. III encompasses the problem formulation and solution. Section IV gives the performance evaluation and analysis, followed by the conclusion and future outlook.

II. RSMA-mMIMO-xURLLC NETWORK ARCHITECTURE

As illustrated in Fig. 1, we examine a downlink RSMA-mMIMO-xURLLC network architecture, where a base station (BS) equipped with N_T antennas concurrently serves U user equipments (UEs) equipped with N_R antennas ($N_T \gg N_R$). Each UE u requests message M_u from BS, where $u \in \mathcal{U} \triangleq \{1, \dots, U\}$. Following RSMA principles [6, 7], M_u is split into a common message M_u^c and a private message M_u^p . All

common messages $\{M_1^c, \dots, M_U^c\}$ are combined into a super-common message M_c , encoded into a common stream s_c . The codebook of s_c is shared with all receivers to ensure successful decoding of s_c . Conversely, each M_u^p is independently encoded into a private stream s_u^p , with its codebook shared solely with its designated receiver $u \in \mathcal{U}$. Subsequently, streams $\mathbf{s} \triangleq [s_1^p, \dots, s_U^p, s_c]^T \in \mathbb{C}^{(U+1) \times 1}$, $\mathbb{E}[\mathbf{s}\mathbf{s}^H] = \mathbf{I}$ are precoded into transmitted signals $\mathbf{x} \triangleq [x_1, \dots, x_{N_T}]^T$ through linear precoding, where x_i denotes the signal corresponding to the i -th transmit antenna ($i = 1, \dots, N_T$).

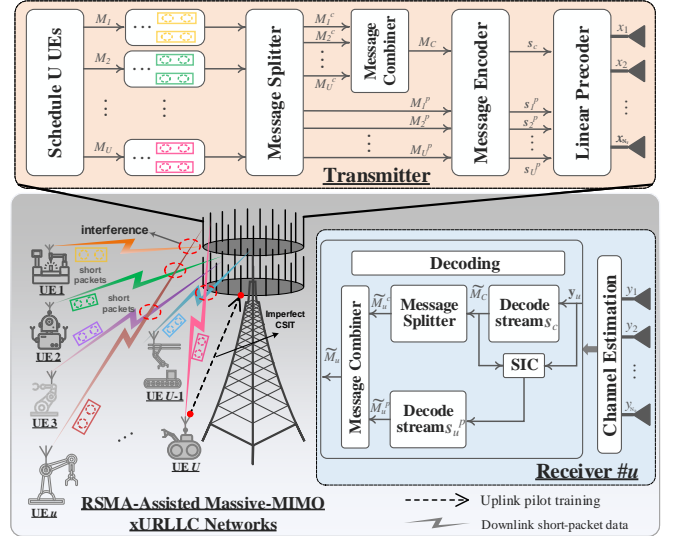


Fig. 1: The RSMA-assisted massive-MIMO xURLLC network architecture.

A. Critical QoS Provisioning Requirements for xURLLC

To fulfill the extremely low latency for xURLLC, short-packet data transmission under FBL regimes is mandated to guarantee compliance with low-latency prerequisites [3, 9, 27]. In this context, the maximum achievable rate for multi-antenna receivers can be given by

$$R(N_d, \mathbf{\Gamma}, \varepsilon) \approx \sum_{j=1}^{N_R} \left(\log_2(1 + \Gamma^{(j)}) - \sqrt{\frac{\mathcal{V}(\Gamma^{(j)}) Q^{-1}(\varepsilon)}{N_d \ln 2}} \right), \quad (1)$$

where $\Gamma^{(j)}$ represents the SINR received by the j -th antenna of the receiver, N_d indicates the allocated channel uses (CUs) for xURLLC's short-packet data transmission, ε represents DEP, $Q^{-1}(x)$ symbolizes the inverse of the Q-function, and $\mathcal{V}(\Gamma^{(j)}) = 1 - (1 + \Gamma^{(j)})^{-2}$ characterizes the channel dispersion. Then, the expression of DEP can be expressed as

$$\varepsilon(N_d, \mathbf{\Gamma}, R) = Q(g(N_d, \mathbf{\Gamma}, R)), \quad (2)$$

where

$$g(N_d, \mathbf{\Gamma}, R) = \ln 2 \left(\sum_{j=1}^{N_R} \log_2(1 + \Gamma^{(j)}) - R \right) \left(\sum_{j=1}^{N_R} \sqrt{\frac{\mathcal{V}(\Gamma^{(j)})}{N_d}} \right)^{-1}.$$

Let D_{th} and ε_{th} characterize xURLLC's QoS requirements for latency and reliability, respectively [2–4]. Given the system bandwidth B_{tot} , the symbol duration and the total CUs can be represented by $T_f = 1/B_{tot}$ and $N_{tot} = D_{th}/T_f$, respectively. Under FBL regimes, the short-packet data communications must be accomplished within N_d CUs. As a result, the latency constraint of xURLLC is formulated as $N_d \leq N_{tot} - N_p$, where N_p is the CUs allocated for pilot training, and the reliability constraint can be formulated as $\varepsilon(N_d, \mathbf{\Gamma}, R) \leq \varepsilon_{th}$.

B. Uplink Pilot Training for Channel Estimations

Let $\boldsymbol{\varphi} = [\varphi_1, \dots, \varphi_{N_p}] \in \mathbb{C}^{1 \times N_p}$ denote the orthogonal pilot sequence satisfying $\|\boldsymbol{\varphi}\|^2 = 1$, where operator $\|\cdot\|$ indicates the Euclidean norm ($N_p > N_R$). The uplink pilot signal from UE u to the BS can be represented as $\mathbf{x}_u^{(p)} = \sqrt{N_p} \boldsymbol{\varphi}$ [28]. Let ρ_p represent the transmit power for uplink pilot training, then the received pilot signal of the i -th receive antenna is given by

$$\mathbf{Y}_{u,i}^{(p)} = \sqrt{N_p} \mathbf{g}_{u,i} \mathbf{x}_u^{(p)} + \mathbf{N}^{(p)} = \sqrt{N_p \rho_p} \mathbf{g}_{u,i} \boldsymbol{\varphi} + \mathbf{N}^{(p)}, \quad (3)$$

where $\mathbf{N}^{(p)} \in \mathbb{C}^{N_R \times N_p}$ indicates the additive white Gaussian noise (AWGN) matrix, $\mathbf{g}_{u,i} = \sqrt{\kappa_u} \mathbf{h}_{u,i}$ denotes the channel gain between the UE u and the i -th transmit antenna over the transmitter, where $\kappa_u = [\lambda / (4\pi d_u)]^2$ and λ are the large-scale fading coefficient and the wavelength, respectively. While d_u and $\mathbf{h}_{u,i} \in \mathbb{C}^{N_R \times 1}$ represents the distance and the small-scale fading coefficient between the UE u and the i -th transmit antenna, respectively. The BS undertakes the de-spreading scheme to the received uplink pilot signal [28], which can be given by (4) after the de-spreading operation:

$$\bar{\mathbf{y}}_{u,i}^{(p)} = \mathbf{Y}_{u,i}^{(p)} \boldsymbol{\varphi}^H = \sqrt{N_p \rho_p} \mathbf{g}_{u,i} + \bar{\mathbf{n}}^{(p)} \quad (4)$$

where each element of $\bar{\mathbf{n}}^{(p)} \in \mathbb{R}^{N_R \times 1}$ follows the Gaussian distribution $\mathcal{N}(0, 1)$. Let $\hat{\mathbf{G}}_u = [\hat{\mathbf{g}}_{u,1}, \dots, \hat{\mathbf{g}}_{u,N_T}] \in \mathbb{C}^{N_R \times N_T}$ indicate the estimation of the channel gain matrix $\mathbf{G}_u = [\mathbf{g}_{u,1}, \dots, \mathbf{g}_{u,N_T}] \in \mathbb{C}^{N_R \times N_T}$. By exploiting the minimum mean-square error (MMSE) estimation, we have [28]

$$\hat{\mathbf{g}}_{u,i} = \mathbb{E} [\mathbf{g}_{u,i} | \bar{\mathbf{y}}_{u,i}^{(p)}] = \frac{\sqrt{N_p \rho_p \kappa_u}}{1 + N_p \rho_p \kappa_u} \bar{\mathbf{y}}_{u,i}^{(p)}. \quad (5)$$

By substituting (4) into (5), the estimated channel gain $\hat{\mathbf{g}}_{u,i}$ can be given as follows:

$$\hat{\mathbf{g}}_{u,i} = \frac{N_p \rho_p \kappa_u}{1 + N_p \rho_p \kappa_u} \mathbf{g}_{u,i} + \frac{\sqrt{N_p \rho_p \kappa_u}}{1 + N_p \rho_p \kappa_u} \bar{\mathbf{n}}^{(p)} \quad (6)$$

C. Precoder Design for Beamforming

By leveraging RSMA technique [6, 7], the transmitted signal $\mathbf{x} \in \mathbb{C}^{N_T \times 1}$ can be given by

$$\mathbf{x} = \sqrt{\rho_c} \mathbf{w}_c \mathbf{s}_c + \theta \sum_{u=1}^U \sqrt{\rho_{p,u}} \mathbf{w}_{p,u} \mathbf{s}_{p,u}, \quad (7)$$

where θ denotes the parameter that normalizes the total transmit power to 1, ρ_c and $\rho_{p,u}$ are the transmit power allocated for \mathbf{s}_c and $\mathbf{s}_{p,u}$, respectively. While $\mathbf{w}_c \in \mathbb{C}^{N_T \times 1}$ and $\mathbf{W}_p = [\mathbf{w}_{p,1}, \dots, \mathbf{w}_{p,U}] \in \mathbb{C}^{N_T \times U}$ indicate the precoders designed for \mathbf{s}_c and $[\mathbf{s}_{p,1}, \dots, \mathbf{s}_{p,U}]$, respectively. By exploiting the zero-forcing (ZF) precoding scheme, \mathbf{W}_p can be denoted as

$$\mathbf{W}_p = \sqrt{N_T - N_R} \mathbf{Z}^* \left(\mathbf{Z}^T \mathbf{Z}^* \right)^{-1}, \quad (8)$$

where $\mathbf{Z} \in \mathbb{C}^{N_T \times U}$, and the elements of \mathbf{Z} are i.i.d. and follows $\mathcal{CN}(0, 1)$. From (8), the normalized parameter θ can be obtained as follows [29]:

$$\theta = \left(\mathbb{E} \left[\text{Tr} \left((\mathbf{W}_p)^H \mathbf{W}_p \right) \right] \right)^{-\frac{1}{2}} = \sqrt{\frac{(N_T - N_R) N_p \rho_p}{N_R (N_p \rho_p + 1)}}. \quad (9)$$

According to [6, 7, 30], the precoder \mathbf{w}_c for the common stream \mathbf{s}_c can be given as follow:

$$\mathbf{w}_c = \sum_{u=1}^U \xi_u (\hat{\mathbf{g}}_u)^H, \quad (10)$$

where $\hat{\mathbf{g}}_u$ denotes the row vector of $\hat{\mathbf{G}}_u$. Remarkably, since the distances of all antennas on each UE u are very close, we can reasonably have $\mathbf{g}_u^{(j)} \approx \mathbf{g}_u^{(j')} = \mathbf{g}_u$ and $\hat{\mathbf{g}}_u^{(j)} \approx \hat{\mathbf{g}}_u^{(j')} = \hat{\mathbf{g}}_u$ ($\forall j, j' \in \{1, \dots, N_R\}, j \neq j'$), where $\mathbf{g}_u^{(j)}$ and $\hat{\mathbf{g}}_u^{(j)}$ denote the j -th row vector of \mathbf{G}_u and $\hat{\mathbf{G}}_u$, respectively. And the expression of ξ_u can be given by

$$\xi_u = 1 / \sqrt{N_T \sum_{k=1}^U \frac{\pi_u (1 - \varpi_u^2)}{\pi_k (1 - \varpi_k^2)}}, \quad (11)$$

where

$$\varpi_u = \frac{\sqrt{N_p \rho_p \kappa_u}}{1 + N_p \rho_p \kappa_u}, \quad \pi_u = \rho_c \left(\sum_{u=1}^U \rho_{p,u} |\mathbf{g}_u \mathbf{w}_{p,u}|^2 + 1 \right)^{-1}, \quad (12)$$

in which ϖ_u indicates the channel estimation quality of receiver $u \in \mathcal{U}$. When $\varpi_u \rightarrow 0$, it indicates the perfect CSI estimation; while $\varpi_u \rightarrow 1$ denotes that the estimated channel is uncorrelated with the actual channel.

D. Downlink Short-Packet Data Transmission

The received signals corresponding to the j -th antenna over the receiver $u \in \mathcal{U}$ can be given by

$$\begin{aligned} y_u^{(j)} = & \mathbf{g}_u^{(j)} \mathbf{x} + w_u^{(j)} = \underbrace{\sqrt{\rho_c} \mathbf{g}_u^{(j)} \mathbf{w}_c \mathbf{s}_c}_{\text{common message}} + w_u^{(j)} \\ & + \theta \left(\underbrace{\sqrt{\rho_{p,u}} \mathbf{g}_u^{(j)} \mathbf{w}_{p,u} \mathbf{s}_{p,u}}_{\text{private message for UE } u} + \underbrace{\sum_{k=1, k \neq u}^U \sqrt{\rho_{p,k}} \mathbf{g}_u^{(j)} \mathbf{w}_{p,k} \mathbf{s}_{p,k}}_{\text{interference for UE } u} \right), \end{aligned} \quad (13)$$

where $w_u^{(j)}$ denotes the AWGN noise received by the j -th antenna of UE $u \in \mathcal{U}$. Following RSMA principles [6, 7, 30], we first decode the most important common message, which is interfered with by all UEs' private messages. Therefore, the SINR of the common message received by the j -th antenna on UE u is given by

$$\Gamma_{c,u}^{(j)} = \frac{\text{Var} \left[\sqrt{\rho_c} \mathbf{g}_u^{(j)} \mathbf{w}_c \mathbf{s}_c \right]}{\sum_{k=1}^U \text{Var} \left[\sqrt{\rho_{p,k}} \mathbf{g}_u^{(j)} \mathbf{w}_{p,k} \mathbf{s}_{p,k} \right] + 1}. \quad (14)$$

Subsequently, we decode the private message $\mathbf{s}_{p,u}$. If \mathbf{s}_c can be decoded successfully, then $\mathbf{s}_{p,u}$ is interfered with by private messages from other UEs, and the corresponding SINR can be given by

$$\Gamma_{p,u}^{(j)} = \frac{\text{Var} \left[\sqrt{\rho_{p,u}} \mathbf{g}_u^{(j)} \mathbf{w}_{p,u} \mathbf{s}_{p,u} \right]}{\sum_{k=1, k \neq u}^U \text{Var} \left[\sqrt{\rho_{p,k}} \mathbf{g}_u^{(j)} \mathbf{w}_{p,k} \mathbf{s}_{p,k} \right] + 1}. \quad (15)$$

If receiver u fails to decode \mathbf{s}_c , the decoding of $\mathbf{s}_{p,u}$ is interfered with by both \mathbf{s}_c and the private messages of other UEs. In this case, the corresponding SINR is given by

$$\hat{\Gamma}_{p,u}^{(j)} = \frac{\text{Var} \left[\sqrt{\rho_{p,u}} \mathbf{g}_u^{(j)} \mathbf{w}_{p,u} \mathbf{s}_{p,u} \right]}{\text{Var} \left[\sqrt{\rho_c} \mathbf{g}_u^{(j)} \mathbf{w}_c \mathbf{s}_c \right] + \sum_{k=1, k \neq u}^U \text{Var} \left[\sqrt{\rho_{p,k}} \mathbf{g}_u^{(j)} \mathbf{w}_{p,k} \mathbf{s}_{p,k} \right] + 1}. \quad (16)$$

III. PROBLEM FORMULATION AND SOLUTION

A. Problem Formulation

Under FBL regimes [3, 9, 27], the imperfect SIC caused by non-vanishing DEP need to be incorporated. The DEP of receiver u decoding common stream \mathbf{s}_c can be expressed as

$$\varepsilon_{c,u}(N_d, \Gamma_{c,u}, \mathcal{R}_c) = Q(g(N_d, \Gamma_{c,u}, \mathcal{R}_c)), \quad (17)$$

where \mathcal{R}_c indicates the transmission rate of \mathbf{s}_c , and $\mathbf{\Gamma}_{c,u} = [\Gamma_{c,u}^{(1)}, \dots, \Gamma_{c,u}^{(N_R)}]^T$. To guarantee all receivers can successfully decode \mathbf{s}_c , \mathcal{R}_c must fulfill the constraints as follows:

$$\mathcal{R}_c \leq \min_{u \in \mathcal{U}} \{C_{c,u}(N_d, \mathbf{\Gamma}_{c,u}, \varepsilon)\} \leq \min_{u \in \mathcal{U}} \{C_{c,u}(N_d, \mathbf{\Gamma}_{c,u}, \varepsilon_{th})\}, \quad (18)$$

where $C_{c,u}(N_d, \mathbf{\Gamma}_{c,u}, \varepsilon)$ denotes the maximum achievable rate when decoding \mathbf{s}_c , and it can be given by

$$C_{c,u}(N_d, \mathbf{\Gamma}_{c,u}, \varepsilon) = \sum_{j=1}^{N_R} \left(\log_2 \left(1 + \Gamma_{c,u}^{(j)} \right) - \sqrt{\frac{\mathcal{V}(\Gamma_{c,u}^{(j)})}{N_d} Q^{-1}(\varepsilon)} \right). \quad (19)$$

Let $\mathcal{R}_{c,u}$ denote the common rate allocated to receiver $u \in \mathcal{U}$, it satisfies that

$$\sum_{u=1}^U \mathcal{R}_{c,u} \leq \mathcal{R}_c. \quad (20)$$

Combining (17)-(20), the ETR of the common stream \mathbf{s}_c can be given by

$$\tilde{\mathcal{R}}_{c,u} = \mathcal{R}_{c,u} \cdot (1 - \varepsilon_{c,u}(N_d, \mathbf{\Gamma}_{c,u}, \mathcal{R}_c)). \quad (21)$$

If receiver $u \in \mathcal{U}$ successfully decodes \mathbf{s}_c , the DEP of $\mathbf{s}_{p,u}$ can be represented by $\varepsilon_{p,u}(N_d, \mathbf{\Gamma}_{p,u}, \mathcal{R}_{p,u})$. If receiver $u \in \mathcal{U}$ fails to decode \mathbf{s}_c , the DEP of $\mathbf{s}_{p,u}$ can be denoted as $\hat{\varepsilon}_{p,u}(N_d, \hat{\mathbf{\Gamma}}_{p,u}, \mathcal{R}_{p,u})$, where $\mathbf{\Gamma}_{p,u} = [\Gamma_{p,u}^{(1)}, \dots, \Gamma_{p,u}^{(N_R)}]^T$ and $\hat{\mathbf{\Gamma}}_{p,u} = [\hat{\Gamma}_{p,u}^{(1)}, \dots, \hat{\Gamma}_{p,u}^{(N_R)}]^T$. $\mathcal{R}_{p,u}$ is the transmission rate allocated to $\mathbf{s}_{p,k}$. Therefore, the ETR of $\mathbf{s}_{p,u}$ is given by

$$\begin{aligned} \tilde{\mathcal{R}}_{p,u} &= \mathcal{R}_{p,u} \cdot (1 - \varepsilon_{c,u} \hat{\varepsilon}_{p,u} - (1 - \varepsilon_{c,u}) \varepsilon_{p,u}) \\ &\approx \mathcal{R}_{p,u} \cdot (1 - \varepsilon_{p,u}(N_d, \mathbf{\Gamma}_{p,u}, \mathcal{R}_{p,u})). \end{aligned} \quad (22)$$

Subsequently, we formulate a joint rate splitting, power allocation, transmit antenna selection, pilot length, and block-length optimization problem to maximize the total ETR while guaranteeing QoS requirements for the developed RSMA-mMIMO-xURLLC network architecture, as follows:

$$\mathcal{P1}: \max_{\{N_p, N_d, N_T, \mathcal{R}, \rho\}} \sum_{u \in \mathcal{U}} \left(\mathcal{R}_{c,u} \cdot (1 - \varepsilon_{c,u}(N_d, \mathbf{\Gamma}_{c,u}, \mathcal{R}_c)) + \mathcal{R}_{p,u} \cdot (1 - \varepsilon_{p,u}(N_d, \mathbf{\Gamma}_{p,u}, \mathcal{R}_{p,u})) \right), \quad (23a)$$

$$\text{s.t. } N_T \leq N_p + N_d \leq N_{tot}, \quad N_p \geq N_T, \quad (23b)$$

$$\varepsilon_{c,u}(N_d, \mathbf{\Gamma}_{c,u}, \mathcal{R}_c) \leq \varepsilon_{th}, \quad \forall u \in \mathcal{U}, \quad (23c)$$

$$\varepsilon_{p,u}(N_d, \mathbf{\Gamma}_{p,u}, \mathcal{R}_{p,u}) \leq \varepsilon_{th}, \quad \forall u \in \mathcal{U}, \quad (23d)$$

$$0 \leq \mathcal{R}_c \leq \min_{u \in \mathcal{U}} \{C_{c,u}(N_d, \mathbf{\Gamma}_{c,u}, \varepsilon_{th})\}, \quad (23e)$$

$$\sum_{u=1}^U \mathcal{R}_{c,u} \leq \mathcal{R}_c, \quad (23f)$$

$$\mathcal{R}_{min} \leq \mathcal{R}_{c,u} + \mathcal{R}_{p,u}, \quad \forall u \in \mathcal{U}, \quad (23g)$$

$$\rho_c + \sum_{u=1}^U \rho_{p,u} \leq \rho_{tot}, \quad (23h)$$

$$\mathcal{R}_{c,u} \geq 0, \quad \mathcal{R}_{p,u} \geq 0, \quad \forall u \in \mathcal{U}, \quad (23i)$$

$$\rho_c \geq 0, \quad \rho_{p,u} \geq 0, \quad \forall u \in \mathcal{U}, \quad (23j)$$

where \mathcal{R}_{min} denotes the minimum transmission rate requirement for each receiver, and $\boldsymbol{\rho} = [\rho_c, \rho_{p,1}, \dots, \rho_{p,U}]^T$ and $\mathcal{R} = [\mathcal{R}_c, \mathcal{R}_{p,1}, \dots, \mathcal{R}_{p,U}]^T$. (23b) delineates the latency constraints. (23c) and (23d) indicate the reliability constraints

for receiver $u \in \mathcal{U}$ when delivering the common and private messages, respectively. (23e) and (23f) jointly define the constraints on common transmission rates; (23g) specifies the minimum transmission rate constraints for receivers, and (23h) ensures compliance with the total transmit power constraint.

B. Problem Reformulation

The solution of $\mathcal{P1}$ involves intricately intertwined joint optimization of N_p , N_d , N_T , \mathcal{R} , and $\boldsymbol{\rho}$, leading to a non-convex objective function (23a). This poses $\mathcal{P1}$ becomes a formidable problem, rendering its optimal solution exceedingly challenging. For this reason, it is essential to excavate the intrinsic properties of $\mathcal{P1}$ to simplify and transform $\mathcal{P1}$. **Lemma 1** is elucidated to tackle this challenge.

Lemma 1. *Assuming receivers are uniformly distributed within the cell with an inner radius of R_{min} and an outer radius of R_{max} . The BS is located at a height \tilde{h} , satisfying $\tilde{h} \ll R_{min}$ and $\tilde{h} \ll R_{max}$. Then, we can derive that*

$$\tilde{\Pi}_1 = \frac{\lambda^2 (X_{max}^{(1)} - X_{min}^{(1)})}{(4\pi)^2 (R_{max}^2 - R_{min}^2)}, \quad \tilde{\Pi}_2 = \frac{\lambda^2 \log \left(\frac{X_{max}^{(1)}}{X_{min}^{(1)}} \right)}{(4\pi)^2 (R_{max}^2 - R_{min}^2)}, \quad (24)$$

where

$$\begin{cases} X_{min}^{(1)} = \frac{\lambda^2}{(4\pi)^2 (R_{max}^2 + \tilde{h}^2) + N_p \rho_p \lambda^2}, \\ X_{max}^{(1)} = \frac{\lambda^2}{(4\pi)^2 (R_{min}^2 + \tilde{h}^2) + N_p \rho_p \lambda^2}. \end{cases}$$

$$\tilde{\Pi}_3 = \begin{cases} \frac{\lambda^2 \log \left(\frac{R_{max}}{R_{min}} \right)}{8(\pi N_p \rho_p)^2 (R_{max}^2 - R_{min}^2)}, & N_p \rho_p \kappa_u \gg 1; \\ \frac{\lambda^6 (R_{max}^2 + R_{min}^2)}{2(4\pi)^6 R_{max}^4 R_{min}^4}, & 0 < N_p \rho_p \kappa_u \ll 1; \\ \frac{\lambda^6 (R_{max}^2 + R_{min}^2)}{8(4\pi)^6 R_{max}^4 R_{min}^4}, & N_p \rho_p \kappa_u \approx 1. \end{cases} \quad (25)$$

$$\tilde{\Pi}_4 = \begin{cases} \frac{\lambda^6 (R_{max}^2 + R_{min}^2)}{(4\pi)^6 (N_p \rho_p)^3 R_{max}^4 R_{min}^4}, & N_p \rho_p \kappa_u \gg 1; \\ \frac{\lambda^8}{3(4\pi)^8 (R_{max}^2 - R_{min}^2)} \left(\frac{1}{R_{min}^6} - \frac{1}{R_{max}^6} \right), & 0 < N_p \rho_p \kappa_u \ll 1; \\ \frac{\lambda^8}{12(4\pi)^8 (R_{max}^2 - R_{min}^2)} \left(\frac{1}{R_{min}^6} - \frac{1}{R_{max}^6} \right), & N_p \rho_p \kappa_u \approx 1. \end{cases} \quad (26)$$

$$\tilde{\Pi}_5 = \begin{cases} \frac{\lambda^2 \log \left(\frac{R_{max}}{R_{min}} \right)}{8\pi^2 N_p \rho_p (R_{max}^2 - R_{min}^2)}, & N_p \rho_p \kappa_u \gg 1; \\ \frac{\lambda^6 (R_{max}^2 + R_{min}^2)}{(4\pi)^6 (N_p \rho_p)^3 R_{max}^4 R_{min}^4}, & 0 < N_p \rho_p \kappa_u \ll 1; \\ \frac{\lambda^6 (R_{max}^2 + R_{min}^2)}{2(4\pi)^6 (N_p \rho_p)^3 R_{max}^4 R_{min}^4}, & N_p \rho_p \kappa_u \approx 1; \end{cases} \quad (27)$$

where

$$\tilde{\Pi}_1 = \mathbb{E} \left[\frac{\kappa_u^2}{(1 + N_p \rho_p \kappa_u)^2} \right], \quad \tilde{\Pi}_2 = \mathbb{E} \left[\frac{\kappa_u^{3/2}}{1 + N_p \rho_p \kappa_u} \right], \quad \tilde{\Pi}_3 = \mathbb{E} \left[\frac{\kappa_u^3}{(1 + N_p \rho_p \kappa_u)^2} \right],$$

$$\tilde{\Pi}_4 = \mathbb{E} \left[\frac{\kappa_u^4}{(1 + N_p \rho_p \kappa_u)^2} \right], \quad \text{and} \quad \tilde{\Pi}_5 = \mathbb{E} \left[\frac{\kappa_u^2}{1 + N_p \rho_p \kappa_u} \right].$$

Proof. The proof of **Lemma 1** is given in Appendix A. \square

Using **Lemma 1**, **Theorem 2** is further derived as follows:

Theorem 1. *Under the proposed zero-forcing precoding scheme, the closed-form expressions for the SINR of common and private messages corresponding to (14), (15), and (16) can be transformed into the following forms:*

$$\Gamma_{c,u}^{(j)} = \frac{\rho_c \kappa_u \Psi}{\kappa_u \Psi \sum_{k=1}^U \rho_{p,k} + 1} \approx \frac{\rho_c}{\sum_{k=1}^U \rho_{p,k}}, \quad (28a)$$

$$\Gamma_{p,u}^{(j)} = \frac{\rho_{p,u} \kappa_u \Psi}{\kappa_u \Psi \sum_{k=1, k \neq u}^U \rho_{p,k} + 1} \approx \frac{\rho_{p,u}}{\sum_{k=1, k \neq u}^U \rho_{p,k}}, \quad (28b)$$

$$\hat{\Gamma}_{p,u}^{(j)} = \frac{\rho_{p,u} \kappa_u \Psi}{\kappa_u \Psi \sum_{k=1, k \neq u}^U \rho_{p,k} + \rho_c \kappa_u \Psi + 1} \approx \frac{\rho_{p,u}}{\sum_{k=1, k \neq u}^U \rho_{p,k} + \rho_c}, \quad (28c)$$

where the expression of Ψ can be given by (35).

Proof. According to (14), we can expand $\text{Var} \left[\sqrt{\rho_c} \mathbf{g}_u^{(j)} \mathbf{w}_c \mathbf{s}_c \right]$ into the form described in (29), where (a) can be directly obtained by substituting (10), (b) is easily derived by substituting (6), and (c) is obtained from the property of independent random variables X and Y , namely, $\mathbb{E}[|X+Y|^2] = \mathbb{E}[|X|^2] + \mathbb{E}[|Y|^2]$. Subsequently, we further expand the two components of $\text{Var} \left[\sqrt{\rho_c} \mathbf{g}_u^{(j)} \mathbf{w}_c \mathbf{s}_c \right]$ in (29), as formulated in (30) and (31), respectively. (d) and (f) are expanded through the distributive law of multiplication, followed by organizing and combining the resulting expressions. (e) and (g) can be derived from (32) and (33), respectively, as follows:

$$\mathbb{E}[F_k^2] = N_p \rho_p \xi_k \bar{h}^2 \mathbb{E} \left[\frac{\kappa_u^2}{(1 + N_p \rho_p \kappa_u)^2} \right], \quad (32a)$$

$$\mathbb{E}[F_k] = \sqrt{N_p \rho_p} \xi_k \bar{h} \mathbb{E} \left[\frac{\kappa_u}{(1 + N_p \rho_p \kappa_u)} \right], \quad (32b)$$

$$\mathbb{E}[D_{k,n}^2] = (N_p \rho_p \xi_k \bar{h})^2 \mathbb{E} \left[\frac{\kappa_u^3}{(1 + N_p \rho_p \kappa_u)^2} \right], \quad (33a)$$

$$\mathbb{E}[D_{k,n}] = N_p \rho_p \xi_k \bar{h} \mathbb{E} \left[\frac{\kappa_u^{3/2}}{1 + N_p \rho_p \kappa_u} \right]. \quad (33b)$$

By substituting (30) and (31) into (29) and rearranging (29) leveraging **Lemma 1**, we can derive that

$$\text{Var} \left[\sqrt{\rho_c} \mathbf{g}_u^{(j)} \mathbf{w}_c \mathbf{s}_c \right] = \rho_c \kappa_u \Psi, \quad (34)$$

where Ψ is given by

$$\begin{aligned} \Psi = & N_T \bar{h}^2 N_p \rho_p \left[\left(\sum_{k=1}^U \xi_k^2 \right) \left[\bar{h}^2 N_p \rho_p \left(\tilde{\Pi}_3 + (N_T - 1) \tilde{\Pi}_4 \right) + N_T \tilde{\Pi}_2 \right] \right. \\ & \left. + \left(\sum_{k=1}^U \sum_{v=1, v \neq u}^U \xi_k \xi_v \right) \left[\bar{h}^2 N_p \rho_p \left(\tilde{\Pi}_1^2 + (N_T - 1) \tilde{\Pi}_5^2 \right) + N_T \tilde{\Pi}_1^2 \right] \right]. \end{aligned} \quad (35)$$

Similarly, we can derive that

$$\sum_{k=1}^U \text{Var} \left[\sqrt{\rho_{p,k}} \mathbf{g}_u^{(j)} \mathbf{w}_{p,k} \mathbf{s}_{p,k} \right] = \kappa_u \Psi \sum_{k=1}^U \rho_{p,k}. \quad (36)$$

By substituting (35) and (36) into (14), we can derive (28a). Similarly, (28b) and (28c) can also be derived. \square

Theorem 2 uncovers the intrinsic interrelationship between SINRs and the transmit power of the decoded and interfering streams, holding the potential to transform complex matrix optimization problems into constant-variable optimization problems. Leveraging **Theorem 2**, $\mathcal{P}1$ can be transformed into $\mathcal{P}2$ as follows:

$$\mathcal{P}2 : \max_{\{N_p, N_d, N_T, \mathbf{R}, \rho\}} \mathcal{T}(N_p, N_d, N_T, \mathbf{R}, \rho) = \sum_{u \in \mathcal{U}} \left(\mathcal{R}_{c,u} \cdot (1 - \varepsilon_{c,u}(N_d, \boldsymbol{\rho}, \mathcal{R}_c)) + \mathcal{R}_{p,u} \cdot (1 - \varepsilon_{p,u}(N_d, \boldsymbol{\rho}, \mathcal{R}_{p,u})) \right), \quad (37a)$$

$$\varepsilon_{c,u}(N_d, \boldsymbol{\rho}, \mathcal{R}_c) + \mathcal{R}_{p,u} \cdot (1 - \varepsilon_{p,u}(N_d, \boldsymbol{\rho}, \mathcal{R}_{p,u})), \quad (37a)$$

$$\text{s.t.} \quad \varepsilon_{c,u}(N_d, \boldsymbol{\rho}, \mathcal{R}_c) \leq \varepsilon_{th}, \forall u \in \mathcal{U}, \quad (37b)$$

$$\varepsilon_{p,u}(N_d, \boldsymbol{\rho}, \mathcal{R}_{p,u}) \leq \varepsilon_{th}, \forall u \in \mathcal{U}, \quad (37c)$$

$$0 \leq \mathcal{R}_c \leq \min_{u \in \mathcal{U}} \{C_{c,u}(N_d, \boldsymbol{\rho}, \varepsilon_{th})\}, \quad (37d)$$

$$(23b), \text{ and } (23f) - (23j). \quad (37e)$$

After reformulating $\mathcal{P}1$, $\mathcal{P}2$ with a more concise form is derived. Nevertheless, tackling $\mathcal{P}2$ remains highly challenging, primarily due to the non-convex nature of $Q(g(N_d, \boldsymbol{\rho}, \varepsilon))$ and the reliability constraints (37b)-(37c). To effectively address $\mathcal{P}2$, an optimality analysis for $\mathcal{P}2$ is conducted.

C. Optimality Analysis

Observing $\mathcal{P}2$ intuitively reveals two key points. Firstly, increasing the allocated split rate deteriorates receivers' DEP performance, potentially violating reliability constraints. Secondly, allocating more transmit power and CUs to uplink pilot training improves the channel estimation quality (i.e., $\bar{w}_u \rightarrow 0$), however, it reduces the information bits available for downlink data transmission. Therefore, it is essential to judiciously allocate the split rate, blocklength, and transmit power to optimally balance the resource overhead between uplink pilot training and downlink short-packet transmissions. Inspired by the above analysis, **Lemma 2** is presented below:

Lemma 2. *The DEP $\varepsilon_{c,u}(N_d, \boldsymbol{\rho}, \mathcal{R}_c) / \varepsilon_{p,u}(N_d, \boldsymbol{\rho}, \mathcal{R}_{p,u})$ strictly decreases with N_d and $\rho_c / \rho_{p,u}$, and strictly increases with $\mathcal{R}_c / \mathcal{R}_{p,u}$.*

Proof. The proof of **Lemma 2** is given in Appendix B. \square

Corollary 1 is derived to reveal the optimal conditions.

Corollary 1. *The reliability constraints (37b) and (37c) are active at the optimal solutions. Moreover, there exists at least one optimal solution such that $N_p = N_T$ holds.*

Proof. The proof of **Corollary 1** is given in Appendix C. \square

According to **Lemma 2** and **Corollary 1**, $\mathcal{P}2$ can be equivalently restated as

$$\tilde{\mathcal{P}}2 : \max_{\{N_T, \mathbf{R}, \rho\}} \mathcal{T}(N_T, \mathbf{R}, \rho), \quad (38a)$$

$$\text{s.t.} \quad \sum_{u=1}^U \mathcal{R}_{c,u} = \mathcal{R}_c, \quad (38b)$$

$$(37b) - (37d), (23g), (23h), (23i), (23j). \quad (38c)$$

Although $\tilde{\mathcal{P}}2$ has been simplified, it remains a highly coupled non-convex optimization problem. In this case, $\tilde{\mathcal{P}}2$ is decoupled into three subproblems: the first one involves power allocation, the second one focuses on rate-splitting optimization, furthermore, building upon the results of **Subproblem I** and **II**, the third one deals with transmit antenna selection.

D. Subproblem I: Power Allocation Optimization

Given the rate-splitting strategy $\bar{\mathbf{R}}$, $\tilde{\mathcal{P}}2$ depends on ρ and N_T . Temporarily disregarding N_T , **Subproblem I** can be formulated as follows:

$$\tilde{\mathcal{P}}2\text{-I} : \max_{\{\rho\}} \mathcal{T}(\bar{\mathbf{R}}, \rho), \quad (39a)$$

$$\text{s.t.} \quad (37b), (37c), (38c), (23j). \quad (39b)$$

$$\begin{aligned} \text{Var} \left[\sqrt{\rho_c} \mathbf{g}_u^{(j)} \mathbf{w}_c \mathbf{s}_c \right] &= \rho_c \mathbb{E} \left[\left| \mathbf{g}_u^{(j)} \mathbf{w}_c \right|^2 \right] = \rho_c \mathbb{E} \left[\left(\sum_{n=1}^{N_T} g_{u,n}^{(j)} w_{c,n} \right)^2 \right] \stackrel{(a)}{=} \rho_c \mathbb{E} \left[\left(\sum_{n=1}^{N_T} g_{u,n}^{(j)} \sum_{k=1}^U \xi_k \hat{g}_{k,n}^{(j)} \right)^2 \right] \stackrel{(b)}{=} \rho_c \mathbb{E} \left[\left(\sum_{n=1}^{N_T} \sum_{k=1}^U g_{u,n}^{(j)} \xi_k \right. \right. \\ &\left. \left. \left[\frac{N_p \rho_p \kappa_k}{1 + N_p \rho_p \kappa_k} g_{k,n}^{(j)} + \frac{\sqrt{N_p \rho_p \kappa_k}}{1 + N_p \rho_p \kappa_k} n_p^{(j)} \right] \right)^2 \right] \stackrel{(c)}{=} \rho_c \mathbb{E} \left[\left(\sum_{n=1}^{N_T} \sum_{k=1}^U g_{u,n}^{(j)} \underbrace{\frac{N_p \rho_p \kappa_k \xi_k}{1 + N_p \rho_p \kappa_k} g_{k,n}^{(j)}}_{D_{k,n}} \right)^2 \right] + \rho_c \mathbb{E} \left[\left(\sum_{n=1}^{N_T} \sum_{k=1}^U g_{u,n}^{(j)} \underbrace{\frac{\sqrt{N_p \rho_p \kappa_k} \xi_k}{1 + N_p \rho_p \kappa_k} n_p^{(j)}}_{F_k} \right)^2 \right] \end{aligned} \quad (29)$$

$$\begin{aligned} \rho_c \mathbb{E} \left[\left(\sum_{n=1}^{N_T} \sum_{k=1}^U g_{u,n}^{(j)} F_k n_p^{(j)} \right)^2 \right] &\stackrel{(d)}{=} \rho_c \sum_{n=1}^{N_T} \sum_{k=1}^U \mathbb{E} \left[\left(g_{u,n}^{(j)} F_k \right)^2 \right] + \rho_c \mathbb{E} \left[\sum_{n=1}^{N_T} \left(g_{u,n}^{(j)} \right)^2 \sum_{k=1}^U \left(F_k \sum_{l=1, l \neq k}^U F_l \right) \right] + \rho_c \mathbb{E} \left[\sum_{n=1}^{N_T} \sum_{k=1}^U g_{u,n}^{(j)} F_k \left(\sum_{t=1, t \neq n}^{N_T} \sum_{l=1}^U g_{u,t}^{(j)} F_l \right) \right] \\ &\stackrel{(e)}{=} \rho_c N_T \kappa_u \bar{h}^2 N_p \rho_p \mathbb{E} \left[\frac{\kappa_u^2}{(1 + N_p \rho_p \kappa_u)^2} \right] \sum_{k=1}^U \xi_k^2 + \rho_c N_T \kappa_u \bar{h}^2 N_p \rho_p \left(\mathbb{E} \left[\frac{\kappa_u}{1 + N_p \rho_p \kappa_u} \right] \right)^2 \sum_{k=1}^U \sum_{v=1, v \neq k}^U \xi_v \xi_v + \rho_c N_T (N_T - 1) \kappa_u \bar{h}^2 N_p \rho_p \times \\ &\quad \left(\mathbb{E} \left[\frac{\kappa_u^2}{(1 + N_p \rho_p \kappa_u)^2} \right] \sum_{k=1}^U \xi_k^2 + \left(\mathbb{E} \left[\frac{\kappa_u}{1 + N_p \rho_p \kappa_u} \right] \right)^2 \sum_{k=1}^U \sum_{v=1, v \neq k}^U \xi_v \xi_v \right). \end{aligned} \quad (30)$$

$$\begin{aligned} \rho_c \mathbb{E} \left[\left(\sum_{n=1}^{N_T} \sum_{k=1}^U g_{u,n}^{(j)} D_{k,n} \right)^2 \right] &\stackrel{(f)}{=} \rho_c \sum_{n=1}^{N_T} \sum_{k=1}^U \mathbb{E} \left[\left(g_{u,n}^{(j)} D_{k,n} \right)^2 \right] + \rho_c \mathbb{E} \left[\sum_{n=1}^{N_T} \left(g_{u,n}^{(j)} \right)^2 \sum_{k=1}^U \left(D_{k,n} \sum_{v=1, v \neq k}^U D_{v,n} \right) \right] + \rho_c \mathbb{E} \left[\sum_{n=1}^{N_T} \sum_{k=1}^U g_{u,n}^{(j)} D_{k,n} \left(\sum_{t=1, t \neq n}^{N_T} \sum_{v=1}^U g_{u,t}^{(j)} D_{v,n} \right) \right] \\ &\stackrel{(g)}{=} \rho_c N_T \kappa_u \bar{h}^4 (N_p \rho_p)^2 \mathbb{E} \left[\frac{\kappa_u^3}{(1 + N_p \rho_p \kappa_u)^2} \right] \sum_{k=1}^U \xi_k^2 + \rho_c N_T \kappa_u \bar{h}^4 (N_p \rho_p)^2 \left(\mathbb{E} \left[\frac{\kappa_u^{3/2}}{1 + N_p \rho_p \kappa_u} \right] \right)^2 \sum_{k=1}^U \sum_{v=1, v \neq k}^U \xi_k \xi_v \\ &\quad + \rho_c N_T (N_T - 1) \kappa_u \bar{h}^4 (N_p \rho_p)^2 \left(\mathbb{E} \left[\frac{\kappa_u^4}{(1 + N_p \rho_p \kappa_u)^2} \right] \sum_{k=1}^U \xi_k^2 + \left(\mathbb{E} \left[\frac{\kappa_u^2}{1 + N_p \rho_p \kappa_u} \right] \right)^2 \sum_{k=1}^U \sum_{v=1, v \neq k}^U \xi_k \xi_v \right). \end{aligned} \quad (31)$$

Lemma 3. The function $g(N_d, \Gamma, R)$ is a monotonically increasing concave function with respect to Γ .

Proof. The proof of **Lemma 3** is given in Appendix D. \square

$\tilde{\mathcal{P}}2$ –I is a non-convex problem since (39a), (37b), and (37c) are non-convex. To effectively tackle this intractable non-convex subproblem, we leverage the SCA technique to handle (39a), (37b), and (37c). Firstly, we introduce auxiliary variables $\mathcal{A} \triangleq [\mathcal{A}_1, \dots, \mathcal{A}_U]^T$ and $\mathcal{B} \triangleq [\mathcal{B}_1, \dots, \mathcal{B}_U]^T$, then $\tilde{\mathcal{P}}2$ –I can be equivalently transformed into $\mathcal{P}3$, as follows:

$$\tilde{\mathcal{P}}3: \max_{\{\mathcal{A}, \mathcal{B}, \rho\}} \sum_{u=1}^U \left(\mathcal{R}_{c,u} (1 - Q(\mathcal{A}_u)) + \mathcal{R}_{p,u} (1 - Q(\mathcal{B}_u)) \right), \quad (40a)$$

$$\text{s.t. } Q(\mathcal{A}_u) \leq \varepsilon_{th}, Q(\mathcal{B}_u) \leq \varepsilon_{th}, \forall u \in \mathcal{U}, \quad (40b)$$

$$\mathcal{A}_u \leq \ln 2 \left(\sum_{j=1}^{N_R} \log_2 (1 + \Gamma_{c,u}^{(j)}) - \bar{\mathcal{R}}_{c,u} \right) \cdot \left(\sum_{j=1}^{N_R} \sqrt{\frac{\mathcal{V}(\Gamma_{c,u}^{(j)})}{N_d}} \right)^{-1}, \quad (40c)$$

$$\mathcal{B}_u \leq \ln 2 \left(\sum_{j=1}^{N_R} \log_2 (1 + \Gamma_{p,u}^{(j)}) - \bar{\mathcal{R}}_{p,u} \right) \cdot \left(\sum_{j=1}^{N_R} \sqrt{\frac{\mathcal{V}(\Gamma_{p,u}^{(j)})}{N_d}} \right)^{-1}, \quad (40d)$$

$$(38c), \text{ and } (23j), \quad (40e)$$

where (40a) is a concave function and (40b) is a convex constraint, as $Q(x)$ is convex for $x > 0$. Nevertheless, (40d) and (40e) are non-convex constraints. Leveraging **Theorem 1** and combining **Lemma 3**, we can further introduce auxiliary variables $\mathcal{C} \triangleq [\mathcal{C}_1, \dots, \mathcal{C}_U]^T$ and $\mathcal{D} \triangleq [\mathcal{D}_1, \dots, \mathcal{D}_U]^T$, and then we have

$$\mathcal{A}_u \leq \frac{\sqrt{N_d} \ln 2}{N_R \sqrt{\mathcal{V}(\mathcal{C}_u)}} \left(N_R \log_2 (1 + \mathcal{C}_u) - \bar{\mathcal{R}}_{c,u} \right), \forall u \in \mathcal{U}, \quad (41)$$

$$\mathcal{B}_u \leq \frac{\sqrt{N_d} \ln 2}{N_R \sqrt{\mathcal{V}(\mathcal{D}_u)}} \left(N_R \log_2 (1 + \mathcal{D}_u) - \bar{\mathcal{R}}_{p,u} \right), \forall u \in \mathcal{U}, \quad (42)$$

where

$$\mathcal{C}_u \leq \Gamma_{c,u}^{(j)} \approx \frac{\rho_c}{\sum_{k=1}^U \rho_{p,k}}, \quad \mathcal{D}_u \leq \Gamma_{p,u}^{(j)} \approx \frac{\rho_{p,u}}{\sum_{k=1, k \neq u}^U \rho_{p,k}}. \quad (43)$$

Constraints (41) and (42) are both convex, however, constraint (43) is non-convex. For this reason, auxiliary variables $\mathcal{E} \triangleq [\mathcal{E}_1, \dots, \mathcal{E}_U]^T$ and $\mathcal{F} \triangleq [\mathcal{F}_1, \dots, \mathcal{F}_U]^T$ are introduced:

$$\mathcal{C}_u \leq \frac{2\rho_c}{\mathcal{E}_u^{[t]}} - \frac{\rho_c \mathcal{E}_u}{(\mathcal{E}_u^{[t]})^2}, \quad (44a)$$

$$\mathcal{E}_u \geq \sum_{k=1}^U \rho_{p,k}, \quad (44b)$$

$$\mathcal{D}_u \leq \frac{2\rho_{p,u}}{\mathcal{F}_u^{[t]}} - \frac{\rho_{p,u} \mathcal{F}_u}{(\mathcal{F}_u^{[t]})^2}, \quad (44c)$$

$$\mathcal{F}_u \geq \sum_{k=1, k \neq u}^U \rho_{p,k}, \quad (44d)$$

where constraints (44a)–(44d) are all convex, and operator $[t]$ indicates the t -th iteration of the SCA method.

Combining (39)–(44), $\tilde{\mathcal{P}}2$ –I can be finally equivalently reformulated as follows:

$$\tilde{\mathcal{P}}4: \max_{\{\mathcal{A}, \mathcal{B}, \mathcal{C}, \mathcal{D}, \mathcal{E}, \mathcal{F}, \rho\}} \sum_{u=1}^U \left(\mathcal{R}_{c,u} (1 - Q(\mathcal{A}_u)) + \mathcal{R}_{p,u} (1 - Q(\mathcal{B}_u)) \right), \quad (45a)$$

s.t. (41), (42), (44a) – (44d), (38c), and (23j). (45b)

$\tilde{\mathcal{P}}4$ is convex and can be efficiently solved using interior-point methods. The detailed solution process for **Subproblem I** is summarized as **Algorithm 1**.

Algorithm 1: SCA-based Algorithm for Solving Subproblem I.

Input: $\bar{\mathcal{R}} \triangleq \{\bar{\mathcal{R}}_c, \bar{\mathcal{R}}_{c,1}, \dots, \bar{\mathcal{R}}_{c,U}\}$ and N_d ;
1 Initialize: $\mathcal{A}^{[0]}, \mathcal{B}^{[0]}, \mathcal{C}^{[0]}, \mathcal{D}^{[0]}, \mathcal{E}^{[0]}, \mathcal{F}^{[0]}, \rho^{[0]}$;
2 Set iteration index $t = 0$;
3 while *Convergence Unsatisfied* **do**
4 Use $\mathcal{A}^{[t]}, \mathcal{B}^{[t]}, \mathcal{C}^{[t]}, \mathcal{D}^{[t]}, \mathcal{E}^{[t]}, \mathcal{F}^{[t]}, \rho^{[t]}$ to solve convex problem $\tilde{\mathcal{P}}4$;
5 Obtain the optimal solution of $\tilde{\mathcal{P}}4$:
 $\mathcal{A}^{[t+1]}, \mathcal{B}^{[t+1]}, \mathcal{C}^{[t+1]}, \mathcal{D}^{[t+1]}, \mathcal{E}^{[t+1]}, \mathcal{F}^{[t+1]}, \rho^{[t+1]}$;
6 Set iteration index $t = t + 1$;
7 end
Output: Optimal power allocation strategy $\rho^* = \rho^{[t]}$.

E. Subproblem II: Rate-Splitting Optimization

Given power allocation strategy $\bar{\rho} \triangleq [\bar{\rho}_c, \bar{\rho}_{p,1}, \dots, \bar{\rho}_{p,U}]^T$, $\tilde{\mathcal{P}}2$ only depends on \mathcal{R} and N_T . Similarly, temporarily disregarding N_T , **Subproblem II** can be formulated as follows:

$$\tilde{\mathcal{P}}2\text{--II}: \max_{\{\mathcal{R}\}} \mathcal{T}(\mathcal{R}, \bar{\rho}) = \mathcal{T}_c(\mathcal{R}_c) + \mathcal{T}_p(\mathcal{R}_p), \quad (46a)$$

$$\text{s.t.} \quad (23g), (23i), (37b) - (37d), (38b) \quad (46b)$$

where $\mathcal{R}_c \triangleq [\mathcal{R}_c, \mathcal{R}_{c,1}, \dots, \mathcal{R}_{c,U}]^T$, $\mathcal{R}_p \triangleq [\mathcal{R}_{p,1}, \dots, \mathcal{R}_{c,U}]^T$, and

$$\mathcal{T}_c(\mathcal{R}_c) = \sum_{u=1}^U \mathcal{R}_{c,u} (1 - \varepsilon_{c,u}(\bar{\rho}, \mathcal{R}_c)), \quad (47a)$$

$$\mathcal{T}_p(\mathcal{R}_p) = \sum_{u=1}^U \mathcal{R}_{p,u} (1 - \varepsilon_{p,u}(\bar{\rho}, \mathcal{R}_{p,u})). \quad (47b)$$

Since $\varepsilon_{c,u}$ and $\varepsilon_{p,u}$ are only dependent to \mathcal{R}_c and $\mathcal{R}_{p,u}$, (37a) and (37b) can be transformed into linear constraints. From $\varepsilon_{c,u} \leq \varepsilon_{th}$ and $\varepsilon_{p,u} \leq \varepsilon_{th}$, we can obtain that

$$0 < \mathcal{R}_c \leq \min_{\{u \in \mathcal{U}\}} \{C_{c,u}(N_d, \bar{\rho}, \varepsilon_{th})\} = \mathcal{R}_c^\uparrow, \quad (48a)$$

$$0 < \mathcal{R}_{p,u} \leq \sum_{j=1}^{N_R} \left(\log_2(1 + \Gamma_{p,u}^{(j)}) - \sqrt{\frac{\mathcal{V}(\Gamma_{p,u}^{(j)})}{N_d} \frac{Q^{-1}(\varepsilon_{th})}{\ln 2}} \right) \quad (48b)$$

$$\stackrel{(a)}{=} N_R \left(\log_2(1 + \bar{\Gamma}_{p,u}) - \sqrt{\frac{\mathcal{V}(\bar{\Gamma}_{p,u})}{N_d} \frac{Q^{-1}(\varepsilon_{th})}{\ln 2}} \right) = \mathcal{R}_{p,u}^\uparrow,$$

where (a) can be derived from Theorem 1. Since $\tilde{\mathcal{P}}2\text{--II}$ remains a non-convex problem, directly solving it is challenging. Observing $\tilde{\mathcal{P}}2\text{--II}$, $\mathcal{T}_c(\mathcal{R}_c)$ and $\mathcal{T}_p(\mathcal{R}_p)$ are only coupled in (23g). In this case, we propose to decouple $\tilde{\mathcal{P}}2\text{--II}$ leveraging sequential optimization technique as follows:

$$\tilde{\mathcal{P}}5: \mathcal{R}_p^* = \arg \max_{\{\mathcal{R}_p\}} \mathcal{T}_p(\mathcal{R}_p), \quad (49a)$$

$$\text{s.t.} \quad (48b). \quad (49b)$$

$$\tilde{\mathcal{P}}6: \mathcal{R}_c^* = \arg \max_{\{\mathcal{R}_c\}} \mathcal{T}_c(\mathcal{R}_c), \quad (50a)$$

$$\text{s.t.} \quad \mathcal{R}_{c,u} \geq \mathcal{R}_{min} - \mathcal{R}_{p,u}^*, \quad (50b)$$

$$(48a). \quad (50c)$$

According to sequential optimization techniques, $\tilde{\mathcal{P}}5$ must be tackled first, and then proceed to solve $\tilde{\mathcal{P}}6$ using the results obtained from $\tilde{\mathcal{P}}5$. **Lemma 4** shows that $\tilde{\mathcal{P}}5$ is a strictly convex problem that is solved through interior-point methods.

Lemma 4. $\tilde{\mathcal{P}}5$ is a strictly convex problem in $(0, \mathcal{R}_{p,u}^\uparrow)$.

Proof. The proof of **Lemma 4** is given in Appendix E. \square

Subsequently, we focus on addressing $\tilde{\mathcal{P}}6$. Combining (47a), and (50a)-(50c), it can be readily observed that if \mathcal{R}_c is given, the objective function (47a) of $\tilde{\mathcal{P}}6$ becomes a linear function of $\mathcal{R}_{c,u}$, in this case, we can obtain

$$\tilde{\mathcal{P}}7: \max_{\{\mathcal{R}_{c,u}\}_{u \in \mathcal{U}}} \sum_{u \in \mathcal{U}} \tilde{\mathcal{W}}_{c,u} \mathcal{R}_{c,u},$$

$$\text{s.t.} \quad \mathcal{R}_{c,u} \geq \mathcal{R}_{min} - \mathcal{R}_{p,u}^*,$$

$$\sum_{u \in \mathcal{U}} \mathcal{R}_{c,u} = \mathcal{R}_c,$$

where $\tilde{\mathcal{W}}_{c,u} = 1 - \varepsilon_{c,u}(\bar{\rho}, \mathcal{R}_c)$. $\tilde{\mathcal{P}}7$ is a standard linear programming problem, whose optimal solutions are derived leveraging the Lagrange multiplier method, denoted by

$$\mathcal{R}_{c,u}^* = \begin{cases} \mathcal{R}_{c,u}^{max}, & \text{if } \bar{\Gamma}_{c,u} = \max_{k \in \mathcal{U}} \{\bar{\Gamma}_{c,k}\}; \\ \mathcal{R}_{c,u}^{min}, & \text{otherwise,} \end{cases} \quad (52)$$

where $\mathcal{R}_{c,u}^{min} = \max\{\mathcal{R}_{min} - \mathcal{R}_{p,u}^*, 0\}$ and $\mathcal{R}_{c,u}^{max} = \max\{\mathcal{R}_c - \mathcal{R}_{p,u}^*, 0\}$. Then, $\tilde{\mathcal{P}}6$ can be reformulated by using (52), as follow:

$$\tilde{\mathcal{P}}8: \mathcal{R}_c^* = \arg \max_{\{\mathcal{R}_c\}} \left\{ \sum_{k=1, k \neq u} \mathcal{R}_{c,k}^{min} (1 - \varepsilon_{c,k}(\mathcal{R}_c)) + \left(\mathcal{R}_c - \sum_{k=1, k \neq u} \mathcal{R}_{c,k}^{min} \right) (1 - \varepsilon_{c,u}(\mathcal{R}_c)) \right\}, \quad (53a)$$

$$\text{s.t.} \quad 0 < \mathcal{R}_c \leq \mathcal{R}_c^\uparrow. \quad (53b)$$

Lemma 5 provides evidence that $\tilde{\mathcal{P}}8$ is a strictly convex problem, which can be effectively addressed through standard convex optimization algorithms.

Lemma 5. $\tilde{\mathcal{P}}8$ is a strictly convex problem in $(0, \mathcal{R}_c^\uparrow)$.

Proof. The proof of **Lemma 5** is given in Appendix F. \square

F. Joint Power Allocation, Rate Splitting, and Transmit Antenna Selection Optimization Mechanism

Increasing transmit antennas leads to improvements in system performance, capacity, and reliability. Meanwhile, it results in escalated hardware costs, power consumption, complex signal processing, and heightened sensitivity to interference and DEP. As a result, transmit antenna selection becomes a trade-off problem involving convex integer optimization, which can be efficiently solved by the one-dimensional integer search method [3]. Combining Sec. III-D and E, we propose the joint power allocation, rate splitting, and transmit antenna selection (JPRT) optimization algorithm, the detailed description of which is provided in **Algorithm 2**.

G. Optimality and Complexity Analysis

To analyze the optimality of the proposed JPRT optimization algorithm, **Theorem 2** is derived as follows:

Theorem 2. *The proposed JPRT optimization algorithm achieves a progressively improved total ETR in each iteration and eventually converges to a local optimum.*

Proof. As illustrated in Fig. 2, we first analyze the convergence of steps 4 ~ 15 in **Algorithm 2**. In the t -th iteration, we have $N_T^*[n]$. In the case of a given $\rho^{[t]}[n]$, $\mathcal{T}(N_T^*[n], \mathcal{R}^{[t]}[n], \rho^{[t]}[n])[n]$ only depends on $\mathcal{R}^{[t]}[n]$. After performing rate-splitting optimization, we can obtain

$$\mathcal{T}(N_T^*[n], \mathcal{R}^{*[t]}[n], \rho^{[t]}[n])[n] \geq \mathcal{T}(N_T^*[n], \mathcal{R}^{[t]}[n], \rho^{[t]}[n])[n], \quad (54)$$

where $\mathcal{R}^{*[t]}[n]$ indicates the optimal rate-splitting strategy for a given $\rho^{[t]}[n]$ in the t -th iteration. On the other hand, we can also obtain that

$$\mathcal{T}^*(N_T^*[n], \mathcal{R}^{*[t]}[n], \rho^{*[t]}[n])[n] \geq \mathcal{T}(N_T^*[n], \mathcal{R}^{*[t]}[n], \rho^{[t]}[n])[n]. \quad (55)$$

Based on the results obtained in the t -th iteration, we can derive that

$$\mathcal{T}(N_T^*[n], \mathcal{R}^{*[t+1]}[n], \rho^{*[t+1]}[n])[n] \geq \mathcal{T}^*(N_T^*[n], \mathcal{R}^{*[t]}[n], \rho^{*[t]}[n])[n]. \quad (56)$$

After performing power allocation optimization, we can obtain that

$$\begin{aligned} \mathcal{T}^*(N_T^*[n], \mathcal{R}^{*[t+1]}[n], \rho^{*[t+1]}[n])[n] \\ \geq \mathcal{T}(N_T^*[n], \mathcal{R}^{*[t+1]}[n], \rho^{*[t]}[n])[n]. \end{aligned} \quad (57)$$

After repeated iterations, the total ETR progressively increases in each alternating iteration. Ultimately, the total ETR will converge towards a local optimum and reach $\mathcal{T}^*(N_{max}) - \mathcal{T}^*(N_{max} - 1) \leq \Delta_{th}$, where N_{max} and Δ_{th} denote the number of iterations and the convergence criteria, respectively. \square

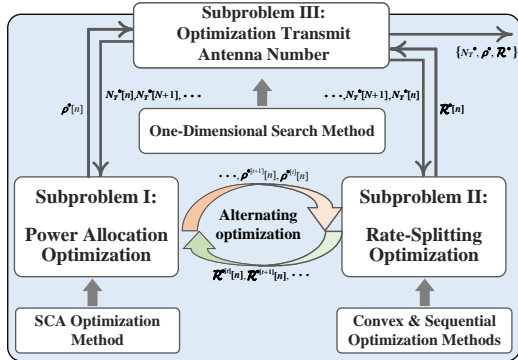


Fig. 2: The illustration of the proposed JPRT optimization mechanism.

The computational complexity of the proposed JPRT optimization algorithm comprises three parts. The first part is power allocation, solved by leveraging the SCA technique, with complexity $\mathcal{O}(N_1 Q)$, where $Q = (7 + N_T)U$ indicates the number of optimization variables updated during each iteration, and $N_1 = \sqrt{2U} + 1 \log_2(1/\epsilon)$ signifies the required iterations [31, 32]. The second part is rate-splitting optimization, where $\tilde{\mathcal{P}}_5$ and $\tilde{\mathcal{P}}_6$ are tackled through interior-point methods, with complexity $\mathcal{O}(U^{3.5} \log_2(1/\epsilon))$ [33]. Finally, the transmit antenna selection optimization, executed post-alternating optimization iterations, is tackled through one-dimensional search methods with complexity $\mathcal{O}(\log_2(N_T^{max}))$ [3, 34]. Therefore, the total computational complexity of **Algorithm 2** can be denoted as $\mathcal{O}\left(\sum_{i=1}^{N_{max}} N_i \sqrt{2} N_T^{*3} U^{3.5} \log_2(1/\epsilon)\right)$, where N_i and $N_{max} \sim \mathcal{O}(\log_2(N_T^{max}))$ are iteration numbers for alternating optimization and transmit antenna selection, respectively.

Algorithm 2: JPRT Optimization Algorithm.

Input: Lower search bound $N_T^{min} = 0$; Upper search bound $N_T^{max} = N_{tot}$;
1 Initialize: Iteration index $n = 1$; $LB[1] = N_T^{min}$;
 $UB[1] = N_T^{max}$;
2 while Convergence-1 Unsatisfied **do**
3 Set $N_T^*[n] = \lfloor (LB[n] + UB[n]) / 2 \rfloor$;
4 Initialize: $\bar{\mathcal{R}}^{*[0]}[n]$, iteration index $t = 0$;
5 while Convergence-2 Unsatisfied **do**
6 // **$\tilde{\mathcal{P}}2$ -I: Power Allocation Optimization**
7 Input $\bar{\mathcal{R}}^{*[t]}[n]$ and $N_T^*[n]$ into **Algorithm 1**;
Execute Algorithm 1 to obtain $\rho^{*[t]}[n]$;
9 // **$\tilde{\mathcal{P}}2$ -II: Rate-Splitting Optimization**
10 Input $\rho^{*[t]}[n]$ and $N_T^*[n]$ into $\tilde{\mathcal{P}}2$ -II;
Solve convex problem $\tilde{\mathcal{P}}5$ to obtain
 $\mathcal{R}_{p,u}^{*[t+1]}[n], \forall u \in \mathcal{U}$;
12 Solve convex problem $\tilde{\mathcal{P}}8$ to obtain $\mathcal{R}_c^{*[t+1]}[n]$;
Substitute $\mathcal{R}_c^{*[t+1]}[n]$ into $\tilde{\mathcal{P}}7$ and solve to obtain
 $\mathcal{R}_{c,u}^{*[t+1]}[n], \forall u \in \mathcal{U}$;
14 Set $\mathcal{R}^{*[t+1]}[n] =$
 $\left[\mathcal{R}_c^{*[t+1]}[n], \mathcal{R}_{c,u}^{*[t+1]}[n], \mathcal{R}_{p,u}^{*[t+1]}[n] \right]^T, \forall u \in \mathcal{U}$;
15 Set $t = t + 1$;
16 end
Set $\rho^*[n] = \rho^{*[t]}[n]$ and $\mathcal{R}^*[n] = \mathcal{R}^{*[t+1]}[n]$;
18 // **Transmit Antenna Selection Optimization**
19 if Convergence-2 Unsatisfied **then**
20 | Set $LB[n + 1] = \lfloor (LB[n] + UB[n]) / 2 \rfloor$;
21 else
22 | Set $UB[n + 1] = \lfloor (LB[n] + UB[n]) / 2 \rfloor$;
23 end
Set $n = n + 1$;
25 end
Output: Optimal Solution $\rho^*[n], \mathcal{R}^*[n], N_T^*[n]$.

TABLE I: Simulation Parameter Settings

| Parameter | Physical meaning | Value |
|---------------------------|---|------------|
| B_{tot} | System bandwidth | 1 MHz |
| $\lambda = \frac{c}{f_c}$ | Wavelength | 15 cm |
| f_c | Carrier frequency | 2 GHz |
| ϵ | Approximate error | 10^{-10} |
| σ^2 | Power of noise | -113 dBm |
| D_{th} | Latency constraint | 1 ms |
| ϵ_{th} | Reliability (Error decoding) constraint | 10^{-5} |
| R_{min} | Minimum distance | 35 m |
| R_{max} | Maximum distance | 95 m |

IV. PERFORMANCE EVALUATION

In this section, extensive numerical results are presented to investigate and demonstrate the superiority, distinctive features, and expansive applicability of the developed RSMA-mMIMO-xURLLC network architecture. In particular, meticulous scrutiny is conducted to assess the technological advancement exhibited by the proposed JPRT optimization algorithm, and several state-of-the-art multiple access techniques are exploited to perform a comprehensive performance comparison. We consider U UEs uniformly distributed within a ring-shaped area around the BS, with distances ranging from $R_{min} = 35$ m to $R_{max} = 95$ m. The small-scale fading is modeled as Rayleigh fading, while the large-scale fading coefficient κ_u can be modeled as $\kappa_u = [\lambda / (4\pi d_u)]^2$, where d_u represents the distance of UE $u \in \mathcal{U}$ from the BS, uniformly distributed within (R_{min}, R_{max}) . Unless explicitly stated otherwise, other simulation parameters are presented in Table I.

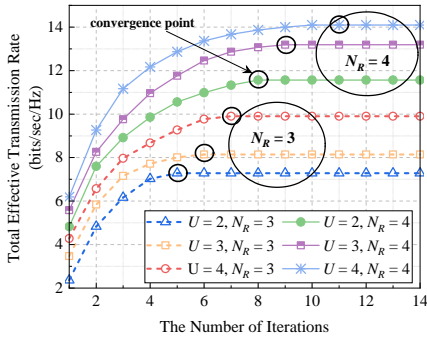


Fig. 3: The convergence behavior of Algorithm 2. $P_{tot} = 4$ W, $N_{tot} = 10^3$ CUs, and $\mathcal{R}_{min} = 2.0$ bits/sec/Hz.

A. Convergence and Optimality Analysis

Fig. 3 illustrates the convergence behavior of the proposed JPRT optimization algorithm. With each iteration, the maximum total ETR progressively increases and rapidly converges, demonstrating **Algorithm 2**'s superior convergence performance and aligning with **Theorem 2**'s theoretical analysis. By maintaining N_R while increasing the number of UEs, the maximum total ETR can be improved. As N_R increases, the maximum total ETR also experiences remarkable gains. These improvements primarily stem from two perspectives. Firstly, our network architecture enables the messages designated for each receiver to be split into common and private parts, and mMIMO systems inherently possess exceptional interference suppression capabilities. Secondly, increasing the number of receiving antennas within mMIMO systems can effectively enhance spatial diversity, which effectively enhances the SINRs of the received signals, thereby improving the total ETR.

As depicted in Fig. 4, the impact of the transmit antenna selection N_T on the maximum total ETR is examined. It can be observed that a discernible tradeoff exists between the total ETR and N_T . Firstly, as N_T increases, the maximum total ETR increases to a peak before gradually declining. The apex of this relationship is marked with pink asterisks * in Fig. 4. When the total transmit power $P_{tot} = 5$ W, the optimal N_T^* increases with blocklength N_{tot} . This is primarily attributed to the constrained power and bandwidth allocated to each CU, and an increase in N_{tot} leads to more intensive utilization of wireless resources, thereby necessitating more N_T to sustain the required SINR and fulfill xURLLC's QoS requirements. Therefore, increasing N_T is beneficial to guarantee stability and reliability during short-packet transmission. Conversely, at $N_{tot} = 900$, the optimal N_T^* decreases with increasing P_{tot} . This is mainly because with the increase of P_{tot} , SINR can be improved, allowing the system to liberate more wireless resources and reduce the number of CUs dedicated to pilot training, thus allocating more channel uses to be allocated to data transmission phase. Consequently, the reduction of the optimal N_T^* can effectively utilize available channel resources, thereby enhancing the total ETR.

Fig. 5 illustrates the relationship between maximum total ETR and xURLLC's QoS requirements (D_{th}, ε_{th}). With fixed ε_{th} , the maximum total ETR exhibits an upward trend with the enlargement of D_{th} , albeit at a decreasing rate. Similarly, for constant D_{th} , the maximum total ETR declines rapidly

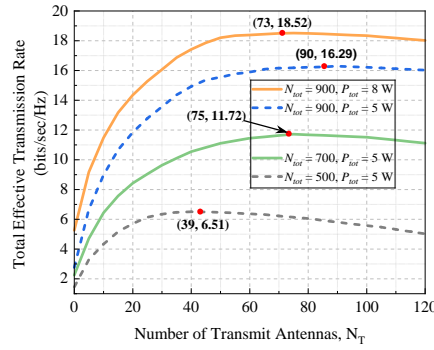


Fig. 4: The optimality performance of Algorithm 2. $U = 5$, $N_R = 4$, and $\mathcal{R}_{min} = 2.0$ bits/sec/Hz.

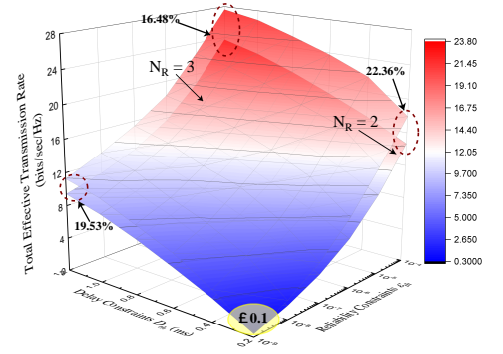


Fig. 5: Maximum ETR versus delay and reliability constraints. $U = 5$, $P_{tot} = 5$ W, and $\mathcal{R}_{min} = 2.0$ bits/sec/Hz.

as ε_{th} decreases, though the descent gradually tapers off. This primarily stems from the fact that as $(D_{th}, \varepsilon_{th})$ relaxes, more resources are available for short-packet data transmission. However, indiscriminately relaxing a particular QoS indicator cannot indefinitely enhance system performance due to strict constraints on blocklength and transmit power. This rationale can be underscored in Fig. 5, where a stringent reliability requirement (e.g., $\varepsilon_{th} = 10^{-9}$) limits performance gains despite latency requirement relaxation (e.g., $D_{th} = 0.2 \sim 1.2$ ms).

B. Comprehensive Performance Comparison

To demonstrate the superior performance of the developed RSMA-mMIMO-xURLLC network architecture, the current state-of-the-art multiple access technologies, i.e., NOMA and SDMA, are selected as benchmarks. RSMA unifies NOMA and SDMA in terms of technical principles under downlink mMIMO scenarios as follows:

- For the NOMA-assisted xURLLC, NOMA can be derived as a sub-scheme of RSMA, leveraging each common stream to fully encode the entire message for individual users [7].
- For SDMA-assisted xURLLC, by prohibiting the power allocation process for all common streams, RSMA seamlessly transforms into SDMA, thereby making SDMA a sub-scheme of all linear precoding-based RSMA [10].

As depicted in Fig. 6, the relationship between the maximum total ETR and the latency constraints is explored. At $N_R = 3$ and $\varepsilon_{th} = 10^{-6}$, our architecture outperforms NOMA and SDMA by approximately 15.3% and 41.91% performance enhancements, respectively, with enhancements growing as D_{th} increases. This underscores our architecture's potential for increased throughput and reduced latency for xURLLC. As D_{th} increases, our network architecture achieves performance gains comparable to NOMA, even under more stringent reliability requirements. This primarily stems from the critical discrepancy between RSMA and NOMA. RSMA can flexibly manage interference by partially decoding it and treating it as noise, softly bridging the two extremes of completely decoding interference and treating interference as noise. Notably, our architecture narrows the performance gaps with SDMA from 81.42% to 4.2% as D_{th} increases from 0.2 ms to 1.2 ms with fewer antennas and stricter reliability requirements. This is mainly because RSMA is the extension of NOMA and SDMA, and it seamlessly integrates with mMIMO systems, striking a balance between optimizing multiplexing and diversity gains.

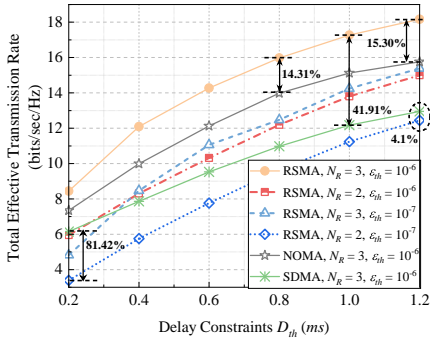


Fig. 6: Maximum ETR versus delay constraints. $U = 5$, $P_{tot} = 5$ W, and $\mathcal{R}_{min} = 2.0$ bits/sec/Hz.

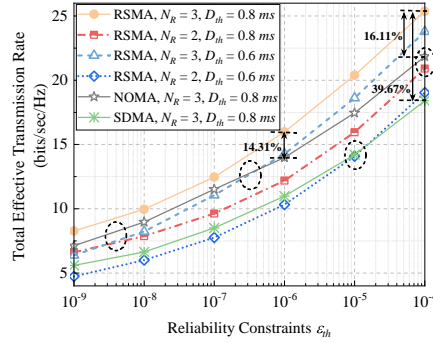


Fig. 7: Maximum ETR versus reliability constraints. $U = 5$, $P_{tot} = 5$ W, and $\mathcal{R}_{min} = 2.0$ bits/sec/Hz.

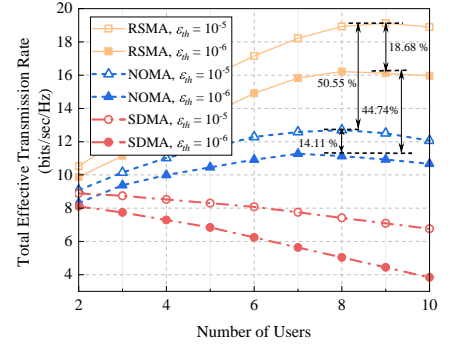


Fig. 8: Relationship between the maximum total ETR and the number of accessed users. $P_{tot} = 5$ W, $N_R = 3$, and $\mathcal{R}_{min} = 2.0$ bits/sec/Hz.

These numerical results substantiate the effectiveness of our architecture in providing enhanced QoS guarantees for xURLLC.

In Fig. 7, we explore the relationship between the maximum total ETR and reliability constraints. At $N_R = 3$ and $D_{th} = 0.8$ ms, our architecture demonstrates around 16.11% and 39.67% performance improvements over NOMA and SDMA, respectively, underscoring its potential to guarantee more stringent reliability constraints for xURLLC. Moreover, as ϵ_{th} increases, our architecture consistently outperforms NOMA, particularly in achieving lower latency, further highlighting its superiority over SDMA. Therefore, similar to the findings in Fig. 6, RSMA exhibits remarkable performance compared to NOMA and SDMA, positioning it as a pivotal technology in 6G networks, poised to meet the stringent QoS requirements.

In Fig. 8, we analyze the relationship between the maximum total ETR and the number of UEs U . Both our architecture and NOMA firstly showcase increased total ETR with U , followed by a decline. Particularly, at $\epsilon_{th} = 10^{-5}$, our developed network architecture peaks at $U > 9$ before declining, while NOMA peaks at $U > 8$. With $\epsilon_{th} = 10^{-6}$, our architecture's peak shifts at $U > 8$, whereas NOMA's peak shifts at $U > 7$. Compared to NOMA, our architecture achieves approximately 55.05% and 44.74% performance gains, respectively, primarily due to differences in SIC decoding mechanisms and interference management strategies. In NOMA, receivers prioritize decoding based on channel conditions. For the receiver with the K -th best channel condition, $U - K$ SIC operations need to be performed. Therefore, the DEPs of receivers with relatively better channel conditions will inevitably be affected by other receivers with relatively poorer channel conditions. Conversely, our architecture integrates RSMA, which only requires one SIC operation at each receiver, significantly reducing the adverse impacts of SIC operations on reliability. Compared with NOMA, our architecture better leverages diversity gains to accommodate more UEs, further demonstrating the RSMA's potential applications in the forthcoming xURLLC. Furthermore, as U increases, the maximum total ETR achievable by SDMA decreases. This is mainly due to SDMA's reliance on spatial division to distinguish signals from different receivers, which can lead to interference between users as the density of UEs increases, thereby affecting transmission rates. Moreover, as wireless resources are inherently limited, an increase in U leads to more frequent resource contention.

Fig. 9 elucidates the relationship between the maximum total

ETR and \mathcal{R}_{min} . It can be intuitively observed that RSMA outperforms NOMA and SDMA, exhibiting slower performance degradation rates. Specifically, when \mathcal{R}_{min} increases from 2.0 to 4.5 bits/Sec/Hz, our architecture only experiences a 41.16% loss in maximum total ETR, while NOMA and SDMA generate losses of approximately 62.99% and 98.92%, respectively. These numerical results demonstrate the robustness of our architecture in maintaining the stability of transmission rates. This is mainly because RSMA can flexibly adjust the transmission rates of common and private messages through rate splitting to accommodate varied \mathcal{R}_{min} . In contrast, NOMA and SDMA are considered two different extreme interference management strategies, with the former completely decoding interference and the latter treating interference as noise. Therefore, NOMA and SDMA lack such adaptability and suffer more significant performance degradation with higher \mathcal{R}_{min} due to their extreme interference management.

In Fig. 10, the relationship between the maximum total ETR and the total transmit power P_{tot} is explored. As expected, the maximum total ETR increases with P_{tot} for all schemes. Moreover, our developed network architecture outperforms NOMA and SDMA. For instance, at $N_R = 4$ and $P_{tot} = 10$ W, the performance gap between RSMA and SDMA is 95.54%. At $N_R = 4$ and $P_{tot} = 11$ W, the performance gains of RSMA exceed NOMA by 32.30%. This is primarily because increasing P_{tot} can enhance the signal strength at receivers, thereby improving channel quality, which in turn reduces DEPs and improves the reliability of short-packet data transmission. Additionally, RSMA's strategy of partial interference decoding and treating interference as noise enables more effective interference management. In contrast, NOMA and SDMA employ simpler interference management strategies, limiting their performance gains.

Fig. 11 illustrates the relationship between maximum total ETR and blocklength N_{tot} , with a target latency $D_{th} = 1$ ms and available bandwidth B_{tot} corresponding to $N_{tot} = 1000 \sim 1800$ CUs, ranging from $B_{tot} = 1.0 \sim 1.8$ MHz. It can be observed that the maximum total ETRs of all three frameworks increase with the N_{tot} , which is consistent with **Corollary 1**. Numerical results reveal that our architecture outperforms NOMA and SDMA, with performance gains expanding as N_{tot} increases. For instance, at $N_{tot} = 1100$ CUs, our architecture achieves approximately 12.09% and 33.06% performance gains compared to NOMA and SDMA, respectively. However, at

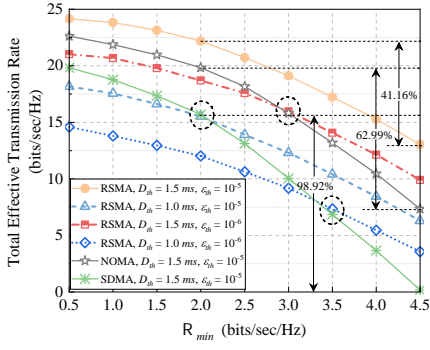


Fig. 9: Relationship between the maximum total ETR and \mathcal{R}_{min} . $U = 5$, $N_R = 3$, and $P_{tot} = 5$ W

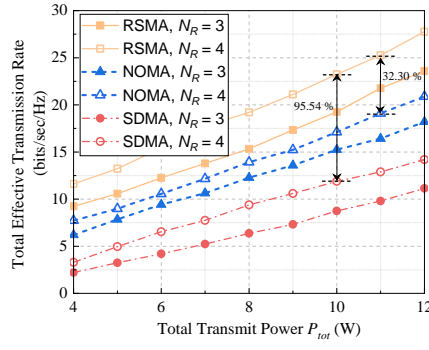


Fig. 10: Relationship between the maximum total ETR and the total transmit power. $U = 5$ and $\mathcal{R}_{min} = 2.0$ bits/Sec/Hz.

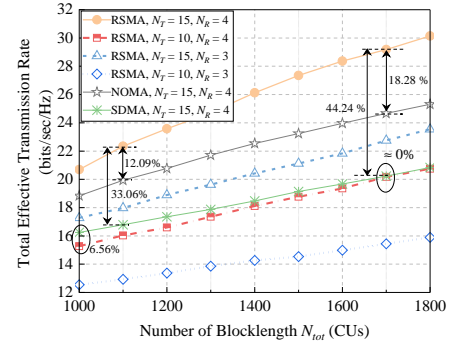


Fig. 11: Relationship between the maximum total ETR and the total blocklength. $U = 5$ and $\mathcal{R}_{min} = 2.0$ bits/Sec/Hz.

$N_{tot} = 1700$ CUs, these improvements expand to 18.28% and 44.24%, respectively. This fully demonstrates our architecture's ability to achieve higher total ETR performance with fewer resources under the identical target delay, which is beneficial for meeting stricter reliability constraints for xURLLC. Furthermore, the robustness of the developed network architecture can also be validated. Even with fewer transmit antennas, our scheme exhibits significant improvements in terms of maximum total ETR performance compared to SDMA.

V. CONCLUSION AND FUTURE OUTLOOK

In this paper, we have embarked on a pioneering exploration for xURLLC's NGAT design and developed an innovative RSMA-mMIMO-xURLLC network architecture to accommodate the critical QoS constraints mandated by xURLLC under imperfect CSIT and FBL regimes. Subsequently, we have formulated a joint rate-splitting, beamforming, and transmit antenna selection optimization problem with the overarching objective of maximizing the total ETR. To effectively tackle this problem, we have reformulated and decomposed it into three subproblems by profoundly exploring the relationships between SINRs of common and private streams and antenna amounts, large-scale fading, transmit power, and blocklength. Moreover, we have proposed a low-complexity JPRT optimization algorithm to efficiently alternate the optimization of these three subproblems. Extensive simulations have substantiated the optimality and exceptional convergence performance of the proposed JPRT optimization algorithm. Compared with the state-of-the-art multi-access schemes, the extraordinary performance of the developed RSMA-mMIMO-xURLLC network architecture has been demonstrated.

In our forthcoming endeavors, we aim to incorporate statistical QoS provisioning mechanisms into the RSMA-mMIMO-xURLLC architecture developed in this paper. This entails a comprehensive analysis of the tail distribution for xURLLC's stringent QoS requirements, thereby endowing our network architecture with enhanced resilience under rare and extreme wireless scenarios.

APPENDIX A PROOF OF LEMMA 1

Given the random variable $R \in (R_{min}, R_{max})$, the p.d.f. of R can be derived owing to the uniform distribution of UEs as follows:

$$p_R(r) = \frac{2r}{R_{max}^2 - R_{min}^2}. \quad (\text{A-1})$$

(i) Define $X_1 = \frac{\kappa_u}{1 + N_p \rho_p \kappa_u}$, the c.d.f. of X_1 can be derived by

$$P_{X_1}(x_1) = \mathbb{P}\{X_1 \leq x_1\} = \mathbb{P}\left\{\frac{\lambda^2}{(4\pi)^2(R^2 + \tilde{h}^2) + N_p \rho_p \lambda^2} \leq x_1\right\} \\ \stackrel{(a)}{=} 1 - \frac{1}{R_{max}^2 - R_{min}^2} \left(\frac{\lambda^2(1 - N_p \rho_p x_1)}{(4\pi)^2 x_1} - \tilde{h}^2 \right), \quad (\text{A-2})$$

where (a) can be derived from (A-1). Taking the derivative with respect to $P_{X_1}(x_1)$, we have

$$p_{X_1}(x_1) = \frac{\partial P_{X_1}(x_1)}{\partial x_1} = \frac{\lambda^2}{(4\pi)^2(R_{max}^2 - R_{min}^2)x_1^2}. \quad (\text{A-3})$$

In this case, we can obtain that

$$\tilde{\Pi}_1 = \mathbb{E}\left[\frac{\kappa_u^2}{(1 + N_p \rho_p \kappa_u)^2}\right] = \mathbb{E}[X_1^2] = \int_{X_{min}^{(1)}}^{X_{max}^{(1)}} x_1^2 p_{X_1}(x_1) dx_1 \\ = \frac{\lambda^2}{(4\pi)^2(R_{max}^2 - R_{min}^2)} \int_{X_{min}^{(1)}}^{X_{max}^{(1)}} \mathbf{1} dx_1 = \frac{\lambda^2(X_{max}^{(1)} - X_{min}^{(1)})}{(4\pi)^2(R_{max}^2 - R_{min}^2)}. \quad (\text{A-4})$$

Similarly, we can also obtain that

$$\tilde{\Pi}_2 = \mathbb{E}\left[\frac{\kappa_u^{3/2}}{1 + N_p \rho_p \kappa_u}\right] \approx \mathbb{E}[X_1] = \frac{\lambda^2 \log\left(\frac{X_{max}^{(1)}}{X_{min}^{(1)}}\right)}{(4\pi)^2(R_{max}^2 - R_{min}^2)}, \quad (\text{A-5})$$

where $X_{min}^{(1)}$ and $X_{max}^{(1)}$ are given by **Lemma 1**.

(ii) We define X_2 as follows:

$$X_2 = \frac{\kappa_u^3}{(1 + N_p \rho_p \kappa_u)^2} = \begin{cases} \frac{\kappa_u}{(N_p \rho_p)^2}, & N_p \rho_p \kappa_u \gg 1; \\ \kappa_u^3, & 0 < N_p \rho_p \kappa_u \ll 1; \\ \frac{\kappa_u^3}{4}, & N_p \rho_p \kappa_u \approx 1. \end{cases} \quad (\text{A-6})$$

When $N_p \rho_p \kappa_u \gg 1$, we can obtain that

$$P_{X_2}(x_2) \stackrel{(a)}{=} 1 - \frac{1}{R_{max}^2 - R_{min}^2} \left(\frac{\lambda^2}{(4\pi N_p \rho_p)^2 x_2} - \tilde{h}^2 \right). \quad (\text{A-7})$$

Taking the derivative with respect to $P_{X_2}(x_2)$, the p.d.f. of X_2 is given by

$$p_{X_2}(x_2) = \frac{\lambda^2}{(R_{max}^2 - R_{min}^2)(4\pi N_p \rho_p)^2 x_2^2}. \quad (\text{A-8})$$

As a result, we can obtain that

$$\tilde{\Pi}_3 = \frac{\lambda^2}{(4\pi N_p \rho_p)^2(R_{max}^2 - R_{min}^2)} \log\left(\frac{R_{max}^2 + \tilde{h}^2}{R_{min}^2 + \tilde{h}^2}\right) \\ \stackrel{(b)}{\approx} \frac{\lambda^2}{8(\pi N_p \rho_p)^2(R_{max}^2 - R_{min}^2)} \log\left(\frac{R_{max}}{R_{min}}\right), \quad (\text{A-9})$$

where (b) indicates that the height of the BS is much smaller than the radius of the cell.

When $0 < N_p \rho_p \kappa_u \ll 1$, the c.d.f. of X_2 can be similarly derived as follows:

$$P_{X_2}(x_2) = 1 - \frac{1}{R_{max}^2 - R_{min}^2} \left(\frac{\lambda^2}{(4\pi)^2 x_2^{1/3}} + \tilde{h}^2 \right). \quad (\text{A-10})$$

By taking the derivative with respect to $P_{X_2}(x_2)$, we have

$$p_{X_2}(x_2) = \frac{\lambda^2}{3(4\pi)^2 (R_{max}^2 - R_{min}^2)} x_2^{-4/3}. \quad (\text{A-11})$$

In this case, we can obtain that

$$\tilde{\Pi}_3 = \frac{\lambda^6 \left[\frac{1}{(R_{min}^2 + \tilde{h}^2)^2} - \frac{1}{(R_{max}^2 + \tilde{h}^2)^2} \right]}{2(4\pi)^6 (R_{max}^2 - R_{min}^2)} \stackrel{(b)}{\approx} \frac{\lambda^6 (R_{max}^2 + R_{min}^2)}{2(4\pi)^6 R_{max}^4 R_{min}^4}. \quad (\text{A-12})$$

Finally, when $N_p \rho_p \kappa_u \approx 1$, according to (A-6) and (A-12), we can directly derive that

$$\tilde{\Pi}_3 \approx \frac{\lambda^6 (R_{max}^2 + R_{min}^2)}{8(4\pi)^6 R_{max}^4 R_{min}^4}. \quad (\text{A-13})$$

Combining (A-9), (A-12), and (A-13), Eq. (25) can be ultimately derived.

(iii) Following a similar derivation process as in (A-6)-(A-13), $\tilde{\Pi}_4$ and $\tilde{\Pi}_5$ can be easily derived, and their closed-form expressions have been presented in (26) and (27), respectively.

APPENDIX B

PROOF OF LEMMA 2

According to [3, 35], we can directly prove that $\varepsilon_{c,u}(N_d, \boldsymbol{\rho}, \mathcal{R}_c)$ and $\varepsilon_{p,u}(N_d, \boldsymbol{\rho}, \mathcal{R}_{p,u})$ are strictly monotone decreasing functions with respect to ρ_c and $\rho_{p,u}$, respectively. Next, we prove that $\varepsilon_{c,u}(N_d, \boldsymbol{\rho}, \mathcal{R}_c)$ is a strictly monotone decreasing function with respect to N_d . Taking partial derivatives w.r.t. N_d for $\varepsilon_{c,u}(N_d, \boldsymbol{\rho}, \mathcal{R}_c)$, we can derive that

$$\begin{aligned} \frac{\partial}{\partial N_d} \varepsilon_{c,u}(N_d, \boldsymbol{\rho}, \mathcal{R}_c) &= \frac{\partial}{\partial N_d} Q(g(N_d, \boldsymbol{\rho}, \mathcal{R}_c)) \\ &= -\frac{N_d^{-\frac{1}{2}}}{2\sqrt{2\pi}} e^{-\frac{g^2(N_d, \boldsymbol{\rho}, \mathcal{R}_c)}{2}} \cdot \left(\frac{\sum_{j=1}^{N_R} \ln(1 + \Gamma_{c,u}^{(j)}) - \mathcal{R}_c \ln 2}{\sum_{j=1}^{N_R} \sqrt{\mathcal{V}(\Gamma_{c,u}^{(j)})}} \right) < 0. \end{aligned} \quad (\text{B-1})$$

From (B-1), we can derive that $\varepsilon_{c,u}(N_d, \boldsymbol{\rho}, \mathcal{R}_c)$ strictly decreases with N_d . Similarly, it can be obtained that $\varepsilon_{p,u}(N_d, \boldsymbol{\rho}, \mathcal{R}_{p,u})$ also monotonically decreases with N_d .

Finally, we show that $\varepsilon_{c,u}(N_d, \boldsymbol{\rho}, \mathcal{R}_c)$ is monotonically increasing with \mathcal{R}_c . Taking partial derivatives w.r.t. \mathcal{R}_c for $\varepsilon_{c,u}(N_d, \boldsymbol{\rho}, \mathcal{R}_c)$, we can derive that

$$\frac{\partial}{\partial \mathcal{R}_c} \varepsilon_{c,u}(N_d, \boldsymbol{\rho}, \mathcal{R}_c) = \frac{\ln 2 \cdot e^{-\frac{g^2(N_d, \boldsymbol{\rho}, \mathcal{R}_c)}{2}}}{\sqrt{2\pi} \sum_{j=1}^{N_R} \mathcal{V}(\Gamma_{c,u}^{(j)})} > 0. \quad (\text{B-2})$$

From (B-2), we can derive that $\varepsilon_{c,u}(N_d, \boldsymbol{\rho}, \mathcal{R}_c)$ strictly increases with \mathcal{R}_c . Similarly, it can be obtained that $\varepsilon_{p,u}(N_d, \boldsymbol{\rho}, \mathcal{R}_{p,u})$ also monotonically decreases with $\mathcal{R}_{p,u}$.

APPENDIX C

PROOF OF COROLLARY 1

We denote the optimal solution of $\mathcal{P}2$ by $\{N_p^\dagger, N_d^\dagger, \mathcal{R}^\dagger, \boldsymbol{\rho}^\dagger\}$. Then, we employ proof by contradiction to show that (37b) always holds. If $\varepsilon_{c,u}(N_d^\dagger, \boldsymbol{\rho}^\dagger, \mathcal{R}_c^\dagger) < \varepsilon_{th}$,

based on **Lemma 2**, we can increase \mathcal{R}_c^\dagger to \mathcal{R}_c^* until $\varepsilon_{c,u}(N_d^\dagger, \boldsymbol{\rho}^\dagger, \mathcal{R}_c^*) = \varepsilon_{th}$ without violating any other constraints, which contradicts the optimality assumption of \mathcal{R}_c^\dagger . As a result, we can conclude that $\varepsilon_{c,u}(N_d, \boldsymbol{\rho}, \mathcal{R}_c) = \varepsilon_{th}$ can be always guaranteed at the optimal solutions. Similarly, we can prove that constraint (37c) is active at the optimal solutions. For constraint (23b), using proof by contradiction, let's assume $N_p^\dagger > N_T$ holds at the optimal solutions. Then, we can decrease N_p^\dagger to $N_p^* = N_T$, and increase ρ_p^\dagger to $\rho_p^* = q\rho_p^\dagger$ with $q = \frac{N_p^\dagger}{N_T} > 1$ such that $N_p^* \rho_p^* = N_p^\dagger \rho_p^\dagger$. It is worth noting that N_d and ρ_p always appear as a product $N_p \rho_p$ in the power constraint (23h). In this case, we have $\mathcal{R}_c^* = \mathcal{R}_c^\dagger$ without violating any other constraints, where \mathcal{R}_c^* is a new transmission rate of common stream under N_p^* and ρ_p^* . This contradicts the optimality of \mathcal{R}_c^\dagger and $N_p^\dagger > N_T$. Therefore, it can be concluded that there exists at least one optimal solution with $N_p = N_T$.

APPENDIX D

PROOF OF LEMMA 3

To prove the monotonic increasing property of $g(N_d, \boldsymbol{\Gamma}, R)$ w.r.t. $\boldsymbol{\Gamma}$, as per (2), it suffices to find the first-order partial derivative of $g(N_d, \boldsymbol{\Gamma}, R)$ w.r.t. $\boldsymbol{\Gamma}$, denoted as $\frac{\partial g}{\partial \boldsymbol{\Gamma}} > 0$. For the concave property of $g(N_d, \boldsymbol{\Gamma}, R)$, we seek the second-order partial derivative of $g(N_d, \boldsymbol{\Gamma}, R)$ w.r.t. $\boldsymbol{\Gamma}$, denoted as $\frac{\partial^2 g}{\partial \boldsymbol{\Gamma}^2} < 0$. The detailed proof process involves only basic rules of differentiation, which readers can validate using tools like Wolfram Mathematica. We omit these steps here.

APPENDIX E

PROOF OF LEMMA 4

According to (47) and (48), for any $u \in \mathcal{U}$, the constraint $\varepsilon_{p,u}(\boldsymbol{\rho}, \mathcal{R}_{p,u}) \leq \varepsilon_{th}$ can be satisfied in $(0, \mathcal{R}_{p,u}^\dagger)$, which is equivalent to $0 < Q^{-1}(\varepsilon_{th}) < g(N_d, \boldsymbol{\Gamma}, \mathcal{R}_{p,u})$. In this case, by taking the second-order partial derivative of $\mathcal{R}_{p,u}$ with respect to $\mathcal{R}_{p,u}$, we can derive that

$$\frac{\partial^2 \tilde{\mathcal{R}}_{p,u}}{\partial \mathcal{R}_{p,u}^2} = -\frac{F_1(\mathcal{R}_{p,u})}{\sqrt{2\pi} \mathcal{V}(\boldsymbol{\Gamma}_{p,u})} \cdot \exp\left\{-\frac{g^2(N_d, \boldsymbol{\Gamma}_{p,u}, \mathcal{R}_{p,u})}{2}\right\} < 0, \quad (\text{E-1})$$

where

$$F_1(\mathcal{R}_{p,u}) = (2 \ln 2) \tilde{\mathcal{V}}(\boldsymbol{\Gamma}_{p,u}) + (\ln 2)^2 \mathcal{R}_{p,u} N_d g(N_d, \boldsymbol{\rho}, \mathcal{R}_{p,u}) > 0, \quad (\text{E-2})$$

in which $\tilde{\mathcal{V}}(\boldsymbol{\Gamma}_{p,u}) = \sqrt{N_d \sum_{j=1}^{N_R} \mathcal{V}(\boldsymbol{\Gamma}_{p,u}^{(j)})}$. Therefore, $\tilde{\mathcal{R}}_{p,u}$ is a strictly convex function w.r.t. $\mathcal{R}_{p,u}$. So, **Lemma 4** can be concluded.

APPENDIX F

PROOF OF LEMMA 5

Similarly, for any $u \in \mathcal{U}$, the constraint $\varepsilon_{c,u}(\boldsymbol{\rho}, \mathcal{R}_{c,u}) \leq \varepsilon_{th}$ can be satisfied in $(0, \mathcal{R}_c^\dagger)$, which is equivalent to $0 < Q^{-1}(\varepsilon_{th}) < g(N_d, \boldsymbol{\Gamma}, \mathcal{R}_c)$. As a result, the second-order partial derivative of $\mathcal{R}_{c,u}$ with respect to $\mathcal{R}_{c,u}$ can be derived as follows:

$$\begin{aligned} \frac{\partial^2 \tilde{\mathcal{R}}_c}{\partial \mathcal{R}_c} &= -\sum_{k=1, k \neq u} \frac{F_2(\mathcal{R}_c)}{\sqrt{2\pi} \mathcal{V}(\boldsymbol{\Gamma}_{c,k})} \cdot \exp\left\{-\frac{g^2(\boldsymbol{\Gamma}_{c,k}, N_d, \mathcal{R}_c)}{2}\right\} \\ &\quad - \frac{\ln 2 \sqrt{N_d} F_3(\mathcal{R}_c)}{\sqrt{2\pi} \mathcal{V}(\boldsymbol{\Gamma}_{c,u})} \cdot \exp\left\{-\frac{g^2(\boldsymbol{\Gamma}_{c,u}, N_d, \mathcal{R}_c)}{2}\right\}, \end{aligned} \quad (\text{F-1})$$

where

$$\begin{cases} F_2(\mathcal{R}_c) = (\ln 2)^2 N_d \mathcal{R}_{c,k}^{\min} g(\Gamma_{c,k}, N_d, \mathcal{R}_c) > 0, \\ F_3(\mathcal{R}_c) = 2\sqrt{\tilde{V}(\Gamma_{c,k})} + \ln 2\sqrt{N_d} \mathcal{R}_{c,k}^{\max} g(\Gamma_{c,k}, N_d, \mathcal{R}_c) > 0, \end{cases}$$

Thus, we can derive that $\frac{\partial^2 \tilde{\mathcal{R}}_c}{\partial \mathcal{R}_c} < 0$, which implies that $\tilde{\mathcal{R}}_c$ is a strictly concave function w.r.t. \mathcal{R}_c in $(0, \mathcal{R}_c^\uparrow)$.

REFERENCES

- [1] J. Park *et al.*, “Extreme ultra-reliable and low-latency communication,” *Nat. Electron.*, vol. 5, no. 3, pp. 133–141, Mar. 2022.
- [2] C. She *et al.*, “A tutorial on ultrareliable and low-latency communications in 6G: Integrating domain knowledge into deep learning,” *Proc. IEEE*, vol. 109, no. 3, pp. 204–246, Mar. 2021.
- [3] Y. Chen *et al.*, “Statistical QoS provisioning analysis and performance optimization in xURLLC-enabled massive MU-MIMO networks: A stochastic network calculus perspective,” *IEEE Trans. Wireless Commun.*, pp. 1–1, 2024.
- [4] Y. Chen *et al.*, “When xURLLC meets NOMA: A stochastic network calculus perspective,” *IEEE Commun. Mag.*, pp. 1–7, 2023.
- [5] Y. Chen, H. Lu, L. Qin, C. Wu, and C. W. Chen, “Streaming 360-degree VR video with statistical QoS provisioning in mmWave networks from delay and rate perspectives,” *arXiv preprint arXiv:2305.07935*, 2023.
- [6] B. Clerckx *et al.*, “A primer on rate-splitting multiple access: Tutorial, myths, and frequently asked questions,” *IEEE J. Sel. Areas Commun.*, 2023.
- [7] Y. Mao *et al.*, “Rate-splitting multiple access: Fundamentals, survey, and future research trends,” *IEEE Commun. Surv. Tutorials*, 2022.
- [8] T. A. Khan *et al.*, “Wirelessly powered communication networks with short packets,” *IEEE Trans. Commun.*, vol. 65, no. 12, pp. 5529–5543, 2017.
- [9] Y. Polyanskiy *et al.*, “Channel coding rate in the finite blocklength regime,” *IEEE Trans. Inf. Theory*, vol. 56, no. 5, pp. 2307–2359, May 2010.
- [10] B. Clerckx *et al.*, “Multiple access techniques for intelligent and multi-functional 6G: Tutorial, survey, and outlook,” 2024.
- [11] Y. Xu *et al.*, “Rate-splitting multiple access with finite blocklength for short-packet and low-latency downlink communications,” *IEEE Trans. Veh. Technol.*, vol. 71, no. 11, pp. 12 333–12 337, 2022.
- [12] Y. Xu *et al.*, “Max-min fairness of rate-splitting multiple access with finite blocklength communications,” *IEEE Trans. Veh. Technol.*, 2022.
- [13] S. Pala *et al.*, “Spectral-efficient RIS-aided RSMA URLLC: Toward mobile broadband reliable low latency communication (mBRLLC) system,” *IEEE Trans. Wireless Commun.*, 2023.
- [14] S. Dey *et al.*, “RSMA in massive MIMO systems: Analysis and optimization in correlated rician-faded channels with phase shifts and aging,” *IEEE Trans. Commun.*, vol. 72, no. 1, pp. 239–256, 2024.
- [15] F. Xiao *et al.*, “Outage performance analysis of RSMA-aided semi-grant-free transmission systems,” *IEEE Open Access J. Commun. Soc.*, vol. 4, pp. 253–268, 2023.
- [16] T. L. Marzetta, “Noncooperative cellular wireless with unlimited numbers of base station antennas,” *IEEE trans. Wireless Commun.*, vol. 9, no. 11, pp. 3590–3600, 2010.
- [17] L. Lu *et al.*, “An overview of massive MIMO: Benefits and challenges,” *IEEE J. Sel. Top. Signal Process.*, vol. 8, no. 5, pp. 742–758, 2014.
- [18] F. Rusek *et al.*, “Scaling up MIMO: Opportunities and challenges with very large arrays,” *IEEE Signal Process. Mag.*, vol. 30, no. 1, pp. 40–60, 2012.
- [19] E. Björnson *et al.*, “Massive MIMO systems with non-ideal hardware: Energy efficiency, estimation, and capacity limits,” *IEEE Trans. Inf. Theory*, vol. 60, no. 11, pp. 7112–7139, 2014.
- [20] E. G. Larsson *et al.*, “Massive MIMO for next generation wireless systems,” *IEEE Commun. Mag.*, vol. 52, no. 2, pp. 186–195, 2014.
- [21] Y. Lin *et al.*, “Joint design of channel training and data transmission for MISO-URLLC systems,” *IEEE Trans. Wireless Commun.*, vol. 21, no. 10, pp. 8646–8659, 2022.
- [22] M. Ke *et al.*, “Next-generation URLLC with massive devices: A unified semi-blind detection framework for sourced and unsourced random access,” *IEEE J. Sel. Areas Commun.*, 2023.
- [23] J. Zhang *et al.*, “Cooperative rate splitting for MISO broadcast channel with user relaying, and performance benefits over cooperative NOMA,” *IEEE Sig. Process. Lett.*, vol. 26, no. 11, pp. 1678–1682, 2019.
- [24] C. Kong and H. Lu, “Cooperative rate-splitting multiple access in heterogeneous networks,” *IEEE Commun. Lett.*, vol. 27, no. 10, pp. 2807–2811, 2023.
- [25] O. Dizdar *et al.*, “Rate-splitting multiple access to mitigate the curse of mobility in (massive) MIMO networks,” *IEEE Trans. Commun.*, vol. 69, no. 10, pp. 6765–6780, 2021.
- [26] H. Jiang *et al.*, “Rate-splitting multiple access for uplink massive MIMO with electromagnetic exposure constraints,” *IEEE J. Sel. Areas Commun.*, vol. 41, no. 5, pp. 1383–1397, 2023.
- [27] W. Yang *et al.*, “Quasi-static multiple-antenna fading channels at finite blocklength,” *IEEE Trans. Inf. Theory*, vol. 60, no. 7, pp. 4232–4265, Jul. 2014.
- [28] T. L. Marzetta *et al.*, *Fundamentals of massive MIMO*. Cambridge University Press, 2016.
- [29] O. Raeesi *et al.*, “Performance analysis of multi-user massive MIMO downlink under channel non-reciprocity and imperfect CSI,” *IEEE Trans. Commun.*, vol. 66, no. 6, pp. 2456–2471, 2018.
- [30] M. Dai *et al.*, “A rate splitting strategy for massive MIMO with imperfect CSIT,” *IEEE Trans. Wireless Commun.*, vol. 15, no. 7, pp. 4611–4624, 2016.
- [31] B. R. Marks and G. P. Wright, “A general inner approximation algorithm for nonconvex mathematical programs,” *Operations research*, vol. 26, no. 4, pp. 681–683, 1978.
- [32] W.-C. Li *et al.*, “Coordinated beamforming for multiuser MISO interference channel under rate outage constraints,” *IEEE Trans. Signal Process.*, vol. 61, no. 5, pp. 1087–1103, 2012.
- [33] S. J. Wright, *Primal-dual interior-point methods*. SIAM, 1997.
- [34] C. Tsai *et al.*, “The golden section search algorithm for finding a good shape parameter for meshless collocation methods,” *Engineering Analysis with Boundary Elements*, vol. 34, no. 8, pp. 738–746, 2010.
- [35] X. Sun *et al.*, “Short-packet downlink transmission with non-orthogonal multiple access,” *IEEE Trans. Wireless Commun.*, vol. 17, no. 7, pp. 4550–4564, 2018.